MEMO 2-20-59E

NASA MEMO 2-20-59E

NASA

MEMORANDUM

A 20,000-KILOWATT NUCLEAR TURBOELECTRIC POWER SUPPLY FOR MANNED SPACE VEHICLES

By Robert E. English, Henry O. Slone, Daniel T. Bernatowicz,

Elmer H. Davison and Seymour Lieblein

Lewis Research Center
Cleveland, Ohio

NATIONAL AERONAUTICS AND SPACE ADMINISTRATION

WASHINGTON

March 1959

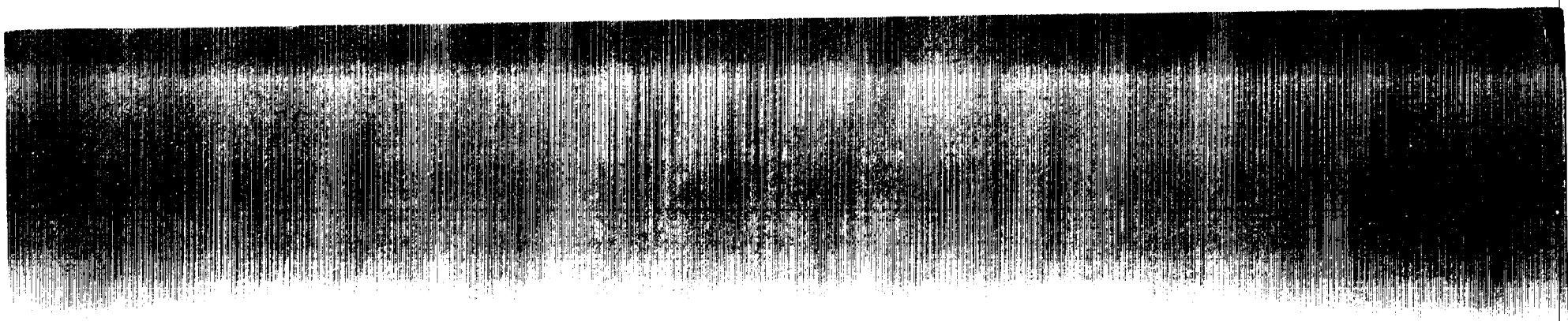

NATIONAL AERONAUTICS AND SPACE ADMINISTRATION

MEMORANDUM 2-20-59E

A 20,000-KILOWATT NUCLEAR TURBOELECTRIC POWER SUPPLY FOR MANNED SPACE VEHICLES

By Robert E. English, Henry O. Slone, Daniel T. Bernatowicz, Elmer H. Davison and Seymour Lieblein

SUMMARY

A conceptual design of a nuclear turboelectric powerplant, producing 20,000 kilowatts of power suitable for manned space vehicles is presented. The study indicates that the radiator necessary for rejecting cycle waste heat is the dominant weight, and emphasis is placed on the selection of cycle operating conditions in order to reduce this weight. A thermodynamic cycle using sodium vapor as the working fluid and operating at a turbine-inlet temperature of 2500° R was selected.

The total powerplant weight was calculated to be approximately 6 pounds per kilowatt. The radiator contributes approximately 2.1 pounds per kilowatt to the total weight and the reactor and reactor shield contribute approximately 0.24 and 1.2 pounds per kilowatt, respectively. The generator, turbine, and piping add significantly to the total weight (between 0.5 and 0.6 lb/kw), but the heat exchanger, pumps, and so on are less important.

Several important research areas associated with the development of a reliable nuclear turboelectric powerplant of the type analyzed are discussed.

INTRODUCTION

Electric power requirements for space applications may range from a few watts to several megawatts, depending on the use. The smaller amounts of power are required for operating instruments and communication equipment. The larger amounts of power are required for electric propulsion in space and some communication equipment. The general purpose of this study is to investigate the characteristics of turbogenerating powerplants presumed suitable for electric propulsion of manned vehicles in space. Only nuclear fission is considered as the source of

heat for the powerplant. The specific purposes of this study are: (1) to investigate the type of turbogenerating powerplant with the greatest potential, (2) to determine the research areas associated with the development of improved powerplants, and (3) to estimate the weight of the powerplant that might be realized per kilowatt of electrical output.

Use of electric power to propel vehicles in space has been considered by a number of investigators; for example, references 1 to 3. Reference 4 proposes a series of measurements requiring small amounts of electrical power. Possible sources of these small amounts of power are surveyed in reference 5.

This report presents the conceptual design of a nuclear turboelectric powerplant using sodium vapor as the cycle working fluid and liquid sodium for the reactor coolant. The analysis was concentrated on an electric power output of 20,000 kilowatts, a level selected in reference 3 as suitable for propulsion of a fairly large manned space vehicle. Powerplants operating on gas and vapor cycles were considered before sodium vapor was selected as the working fluid. Because the early phases of the study indicated that the heaviest single component of a 20,000-kilowatt powerplant would be the radiator required for rejecting waste heat, primary emphasis was placed on the selection of operating conditions to reduce this weight. A specific manned space-vehicle configuration was chosen in order to obtain weight estimates and to make radiation-shielding calculations.

DESCRIPTION OF VEHICLE

In general, each powerplant component is affected by the characteristics of the remainder of the powerplant. Therefore, a general description of the selected powerplant and space-vehicle configuration will serve to clarify the discussion that follows. For some of the powerplant components (such as the radiation shield), the general geometrical configuration of the whole vehicle (not a part of the powerplant proper) must be specified before that component can be analyzed. Since streamlining is unnecessary for space applications, the only requirement for a space vehicle is that there be a convenient and logical arrangement of the various powerplant components and the crew compartment. The vehicle configuration described as follows has some arbitrarily selected features; thus, there are probably other configurations at least as desirable as the one presented here.

The general arrangement of the entire vehicle is shown in figure 1. The crew compartment is at one end of the vehicle, and the reactor and its shield were placed at the opposite end. The structure that ties the reactor and crew compartment together is specified to be rigid so that

Choice of Cycle Working Fluid

Preliminary studies show that the radiator is a significant component (weightwise) at low power levels and becomes the dominating component as the power level is increased. One method for reducing radiator size is to increase the radiator operating temperature. As will be seen later, the minimum radiator area occurs at a relatively fixed value of the ratio of radiator-inlet to turbine-inlet temperature. Therefore, in order to minimize radiator area, increasing the turbine-inlet temperature permits an increase in the temperature of the radiator. In an effort to reduce radiator size, a turbine-inlet temperature of 2500° R was selected for this analysis. It is believed that this value of turbine-inlet temperature might be attained as a result of research and development progress.

In order to choose the best cycle working fluid for the turbogenerating powerplant being analyzed, two basic thermodynamic cycles operating with a turbine-inlet temperature of 2500° R were studied: a gas cycle and a vapor cycle. Both cycles are shown in the temperature-entropy diagram of figure 2. Helium was selected as representative of a gas working fluid, and mercury and sodium were each considered for the vapor cycle.

Although gas and vapor working fluids could be compared in many ways, radiator area was chosen as the appropriate basis for comparison. The equations that relate radiator surface area per kilowatt of electric output and the various cycle parameters are derived in appendix B. (All symbols used in this report are defined in appendix A.) The equation obtained for the gas cycle is

$$\frac{A}{P_e} = \frac{\left(\frac{T_4}{T_3} - \frac{T_1}{T_3}\right)\left[\left(\frac{T_4}{T_3}\right)^2 + \frac{T_1}{T_3}\,\frac{T_4}{T_3} + \left(\frac{T_1}{T_3}\right)^2\right]}{1.53\epsilon\eta_g\left(\frac{T_3}{1000}\right)^4\left(\frac{T_1}{T_3}\right)^3\left(\frac{T_4}{T_3}\right)^3\left\{\left(1 - \frac{T_4}{T_3}\right) - \frac{T_1}{T_3}\,\frac{1}{\eta_C}\left[\frac{\left(\frac{p_2}{p_3}\,\frac{p_4}{p_1}\right)^{\frac{\gamma-1}{\gamma}}}{1 - \frac{1}{\eta_T}\left(1 - \frac{T_4}{T_3}\right)} - 1\right]\right\}} \tag{1}$$

and that obtained for the vapor cycle is

$$\frac{A}{P_e} = \frac{1.972\left(\frac{H_4 - H_1}{H_3 - H_4}\right)}{\epsilon\eta_g\left(\frac{T_4}{1000}\right)^4} \tag{2}$$

it can support compressive as well as tensile loads. Although such a structure is heavier than, say, a pair of cables, the ability of such a structure to withstand compressive loads provides increased confidence that the crew compartment and the reactor will maintain the specified geometrical relation to one another. If the crew compartment moved so that it were no longer in the shadow of the shadow shield, or if it moved toward the reactor, the radiation exposure of the crew would increase.

E-156

The radiator was centrally located (fig. 1), which placed the radiator within the shadow of the reactor shield. The radiator separation from the reactor was a compromise of two factors: Large separation distance (1) decreases the solid angle the shield must occupy and thereby decreases shield weight, and (2) increases the weight of pipes that join the radiator and reactor.

CO-1 back

The vehicle was considered to rotate about its longitudinal axis. This rotation provides artificial gravity for the crew and for free convection within the radiator. Rotation about a line perpendicular to the longitudinal axis was considered and rejected for a number of reasons, most important of which is the fact that the vehicle could not be approached or departed from readily by manned vehicles.

A nominal design life of 750 days of operation at full power was selected. Missions for which such a powerplant might be suitable may be judged by considering that a space vehicle having an initial acceleration of 10^{-4} g could depart from an Earth orbit, descend into an orbit about Mars, and return to an Earth orbit by operating the thrust unit for approximately 250 days (ref. 6). Doubling or halving the design life will not affect the powerplant weight materially.

CYCLE CONSIDERATIONS

General

A typical turbogenerating powerplant using a reactor as the heat source would transfer heat from the reactor to its working fluid, expand the working fluid through a turbine, cool the exhaust gas, and finally complete the cycle by raising the pressure of the working fluid to its initial value. In space, waste heat must be rejected by thermal radiation unless some alternative heat sink can be provided. Use of propellant as a heat sink was considered and rejected for high-specific-impulse electric propulsion systems; the waste heat from the powerplant would require heating even liquid hydrogen to temperatures of the order of $100,000^{\circ}$ R. Thus, heat rejection by thermal radiation seems to be the only suitable method for a turbogenerating powerplant operating in space.

For the turbine-inlet temperature selected for this study (2500° R), equations (1) and (2) were used to determine the minimum radiator areas for the gas and vapor cycles, respectively. Because the gas cycle equation (eq. (1)) contains many parameters, a series of calculations were made to determine the independent effects on radiator area of the individual parameters involved. That is, for fixed values of turbine-inlet temperature T_3 of 2500° R, radiator material emissivity ϵ of 0.90, and the product of generator and mechanical efficiency η_g of 0.95, the remaining parameters in equation (1) were varied. A typical result of such a calculation is shown in figure 3 where the temperature ratios T_4/T_3 (radiator inlet to turbine inlet) and T_1/T_3 (radiator exit to turbine inlet) are permitted to vary for fixed values of compressor and turbine efficiencies ($\eta_C = \eta_T = 0.80$), reactor and radiator pressure ratios $\left(\frac{p_3}{p_2} = \frac{p_1}{p_4} = 0.95\right)$, and a ratio of specific heats γ of 1.66. It is noted on figure 3 that the minimum radiator area occurs for a value of T_4/T_3 of 0.75 and T_1/T_3, approximately 0.30. As each of the other parameters was varied, it was found that the minimum radiator area always occurred at a value of approximately 0.75 for T_4/T_3. Figure 4 indicates the effects of reactor and radiator pressure ratios, compressor and turbine efficiencies, and ratio of specific heats on radiator area. The curves shown on figure 4 are envelope curves obtained from plots such as that shown on figure 3. Note that the abscissa of figure 4 is the minimum cycle temperature (radiator-exit temperature for the gas cycle), T_1, instead of the ratio T_1/T_3, as used on figure 3. As expected, figure 4 shows that the minimum radiator areas for gas cycles require high component efficiencies and minimum pressure losses in the cycle.

The equation relating radiator area per kilowatt and the various vapor-cycle parameters (eq. (2)) is relatively simple to analyze. For fixed values of T_3, ϵ, η_g and a range of values of T_4 (minimum cycle temperature, or radiator-inlet, or -exit temperature), the only variable in equation (2) is turbine efficiency η_T. By varying η_T it was found that the minimum radiator area for the vapor cycle also occurs for a temperature ratio T_4/T_3 of approximately 0.75.

A comparison of the gas and vapor cycles is made in figure 5, in which the variation in radiator surface area per kilowatt with minimum cycle temperature is shown for a turbine-inlet temperature of 2500° R and component efficiencies of 0.80. The helium curve was obtained from figure 4(b) and the vapor curves were calculated from equation (2). The large compressor work penalizes gas cycles by requiring a low temperature entering the radiator. Thermodynamic properties of sodium and mercury were determined as discussed in appendix B.

The two vapor cycles are comparable in radiator area (fig. 5) sodium being slightly better than mercury. However, the minimum radiator areas for a given turbine-inlet temperature are better for vapors than for gases by more than an order of magnitude. Thus, the remainder of this study considers only vapor cycles. The minimum radiator area for these vapor cycles occurs at a radiator temperature of approximately 1900° R. At the temperatures shown in figure 5, there is little to choose between sodium and mercury on a radiator-area bases; however, sodium is superior to mercury because of the pressures involved; that is, at 2500° R, mercury boils at a pressure of approximately 5400 pounds per square inch whereas sodium boils at approximately 75 pounds per square inch. Thus, in the interest of minimizing weight, sodium was chosen as the working fluid for the present application.

Description of Cycle

For a turbine-inlet temperature of 2500° R, a reactor-outlet coolant temperature of 2800° R was selected. Sodium, the cycle working fluid, was selected as the reactor coolant. If the liquid sodium used to cool the reactor is vaporized for use as the cycle working fluid, the reactor shielding problem becomes complicated because the sodium-containing components (turbine, radiator, and pumps) also require shielding. Activation of the working fluid is avoided by introducing an intermediate heat exchanger and using a separate working fluid.

Because of the lack of information on boiling liquid-metal heat transfer it was decided not to boil the working fluid in the intermediate heat exchanger. Instead, the saturated liquid leaving the intermediate heat exchanger is sent to a separator-evaporator. Here the fluid is expanded to high velocity; the concomitant reduction in pressure causes a small fraction of the fluid to evaporate. The high-velocity fluid is directed into a circular path and the centrifugal force separates the vapor and liquid. The vapor then enters the turbine, while the liquid is mixed with the condensate from the radiator and returned to the intermediate heat exchanger.

A temperature-entropy diagram of the cycle chosen for this study is shown in figure 6 and a schematic arrangement is shown in figure 7. Liquid sodium leaves the reactor at 2800° R (200 lb/sq in.) and enters the intermediate heat exchanger. In the intermediate heat exchanger the cycle working fluid is heated to 2700° R (point 5 on fig. 6). In this process, the primary sodium is cooled to 2575° R, and then returned to the reactor. The sodium working fluid from the intermediate heat exchanger enters the separator-evaporator and is expanded to 69 pounds per square inch and a high velocity (point 6 on fig. 6). At this point the fluid is about 4.0 percent vapor. The high-velocity fluid is directed

into a circular path and the centrifugal force separates the vapor and liquid. The vapor (point 3 on fig. 6) then enters the turbine, while the liquid (point 7 on fig. 6) is mixed with the radiator condensate. The working fluid is expanded in the turbine to 2.7 pounds per square inch (saturation temperature, 1800° R; exit quality, 79 percent (point 4 on fig. 6)), producing approximately 360 Btu of work from each pound of sodium passing through the turbine. The working fluid is then condensed in the radiator (to point 1 on fig. 6), its pressure is raised (to point 2 on fig. 6) in the condensate return pump and it is then mixed with the liquid from the evaporator (point 7 on fig. 6). The resulting fluid is at point 8 on figure 6. It is then pumped back into the intermediate heat exchanger (point 9 on fig. 6). The over-all cycle efficiency is approximately 22 percent.

The condensate leaving the radiator is saturated, which may result in cavitation problems in the condensate return pump. If trouble arises, the radiator would have to be enlarged and the fluid subcooled; however, the total heat removed from the working fluid would probably not be increased substantially. The various cycle components will be discussed in following sections.

REACTOR ANALYSIS

The reactor in a space-vehicle powerplant must be small, lightweight, and capable of sustained operation for long periods of time. In the present study, the reactor-outlet coolant temperature is 2800° R. Therefore, the main problem in the design of this reactor is the selection of materials that maintain satisfactory physical properties at high temperatures and yet have acceptable nuclear properties. Another important problem for this application is the large amount of uranium burnup.

For a space-vehicle application, a reactor into which a large amount of fuel beyond the critical investment can be loaded and controlled is desirable so that the reactor requires refuelling as seldom as possible. This burnup consideration and the reactor heat-transfer requirements due to the high power level indicate that the benefits afforded by a hydrogenous moderator (very small critical size and fuel investment) are not exploitable for the present application. Thus, an exchange of improved material physical properties for poorer nuclear properties entails no sacrifice in the reactor design.

Survey of Possible Reactor Types

Some classes of reactors that could be considered for this application are liquid-core and solid-core (homogeneous and heterogeneous) reactors. The liquid-core reactor, that is, one with the fuel dissolved

or dispersed in a liquid moderator, has an inherent advantage for use where a large burnup is required. A liquid core permits extended operation because fuel can be added as it is burned up, and circulation of the liquid can keep the flux and power distributions across the core constant with time. Some of the materials that can be used as liquid moderators, such as molten salts, or aqueous solutions of salts, may be adversely affected by radiation, and some chemical reprocessing and radiolytic gas separation may be needed when these materials are used. However, some liquid metals, mainly beryllium and lithium (separated lithium-7), are good moderators and would not involve the problem of radiation damage. Unfortunately, not much is known about the properties of these liquid metals, especially concerning their compatibility with suitable containment materials at high temperatures.

High-temperature solid-core reactors can be built with more well-known materials. Some materials that are good high-temperature moderators are heavy metal hydrides, graphite, and beryllium oxide. Up to approximately 2000° F some hydrides contain enough hydrogen to be excellent moderators, but there is still the problem of hydrogen diffusing out of the moderator. Graphite has good physical properties at the high temperatures, but its nuclear properties result in very large reactor size. However, beryllium oxide combines both good moderating properties and good physical properties.

Except in low-power reactors, the fuel in solid-core reactors is incorporated in replaceable fuel elements, which contain the coolant flow passages. The maximum allowable fractional burnup of fuel in such elements is limited by the physical damage to the elements due to radiation. Ordinarily, the reactor will have to be shut down and the fuel elements replaced some number of times during the life of the reactor.

Because fuel elements cannot be replaced in a solid-core reactor without shutting down the reactor, a long life in such a reactor can be attained only by large loadings of fuel and high fractional burnup. Even with a liquid-core reactor, where it is possible to add uranium continuously while the reactor is in operation, it might be more convenient to load a great deal of uranium initially. In order to do this, a large amount of controllable negative reactivity is needed. Shim and control rods can be used to control excess reactivity, but the amount is limited by the acceptable flux and power distortions caused by changes in rod positions. The amount of extra fuel that can be controlled can be increased by adding a burnable poison with the fuel. For truly thermal reactors in which there are negligible fissions at energies above thermal, nuclides with thermal absorption cross-sections in the range of 700 to 2500 barns are most promising. Lithium-6, iridium-191, mercury-199 seem to be useful poisons for thermal reactors. When an appreciable number of fissions occur at epithermal and intermediate energies, resonance absorption in the poison becomes important, and an evaluation of the effect of the poisons cannot be made by a simple examination of cross sections.

Reactor Design

Although it was felt that a liquid-core reactor would be well suited to this application, the lack of information mentioned previously precluded any evaluation or design of such a reactor. Therefore, a more conventional reactor, one moderated and reflected by beryllium oxide, was selected for this study.

The discussion of reactor design is organized as follows. First, considerations of reactor heat transfer will determine the reactor dimensions. Then, reactor criticality and fuel element design will be discussed.

Reactor heat transfer. - The calculations of the reactor heat-removal system considered in the present study were of a preliminary nature.

A cylindrical reactor with a length-to-diameter ratio $(L/D)_R$ of 1.0, and a ratio of reactor flow area to reactor cross-sectional area α of 0.30 was selected for this analysis. A flat radial and a cosine axial neutron flux distribution giving a ratio of maximum to average power density of 1.57 (ref. 7, p. 644) was chosen. It was further assumed that the method of heat removal is by forced-convection internal cooling wherein the coolant (liquid sodium) makes one pass through the reactor. The coolant weight flow w and coolant-inlet and -outlet temperatures are specified by the system cycle analysis. For ease in calculations, an equation giving reactor diameter D_R in terms of reactor design variables and coolant properties was obtained as follows:

For a nuclear reactor in which the coolant flows between closely spaced vertical fuel plates having a width B and a spacing between the fuel plates of $d_e/2$, the continuity equation

$$w = \rho A_f V \tag{3}$$

and reactor flow area A_f

$$A_f = N \frac{d_e}{2} B \tag{4}$$

combine to give the number of coolant passages N

$$N = \frac{2w}{\rho d_e B V} \tag{5}$$

The maximum rate of heat transfer to the coolant QF_a^* is

$$QF_a^* = hS_h\theta = hN2BL_R\theta \tag{6}$$

where

$$Q = wc_p \Delta T \tag{7}$$

By combining equations (5), (6), and (7), the following equation results:

$$D_R = \frac{F_a^* c_p \rho V d_e \Delta T}{4h\theta\left(\frac{L}{D}\right)_R} \tag{8}$$

The heat-transfer coefficient h is obtained from the following correlation for liquid metals (ref. 7, p. 679)

$$h = \frac{k}{d_e}\left\{7 + 0.025\left[(Re)(Pr)\right]^{0.8}\right\} \tag{9}$$

Thus, by using the aforementioned assumed and specified variables, and assigning a range of values for d_e, θ, and coolant velocity V, equation (8) determines the required reactor diameter. The value of h was assumed constant along the coolant passage length. For each combination of variables assumed, the reactor pressure drop is obtained from the following relation (ref. 7)

$$\Delta p = \frac{1.5\ \rho V^2}{2g} + \frac{4f\rho V^2 L_R}{2gd} \tag{10}$$

where for turbulent flow,

$$f = 0.079(Re)^{-0.25} \tag{11}$$

The first term in equation (10) accounts for the pressure loss due to contraction and expansion as the coolant enters and leaves the coolant passages, and the second term gives the pressure loss due to fluid friction in the coolant passage.

For an electrical power output of 20,000 kilowatts the cycle analysis dictates that the reactor thermal power is 88,000 kilowatts and the reactor coolant flow and coolant temperature rise are 1235 pounds per second and 225° R, respectively. Using equations (5), (8), and (10), a cylindrical reactor was selected having a diameter and height of 30 inches with approximately 590 coolant passages and a coolant-passage hydraulic diameter of approximately 0.24 inch. The coolant velocity was 22.5 feet per second and the coolant pressure drop was approximately 8 pounds per square inch.

Reactor criticality. - Using the reactor dimensions determined by heat-transfer considerations, and assuming the reactor is reflected on all sides by 3 inches of beryllium-oxide, the critical fuel mass was determined by two-group theory using a reflector savings of 6 inches (twice the actual reflector thickness). In the determination of the group constants it was assumed for convenience that the coolant volume was empty, not filled with sodium as it will be in operation. If the sodium were included in the computations, the moderating properties of the core would be improved but then lower reflector savings should be assumed, and there would be some cancellation of effects. Furthermore, an error in the critical mass has very little effect on the powerplant analysis. The computed critical mass is 21 kilograms and the resonance escape probability is 0.23, indicating that the reactor with this loading is not thermal.

However, a higher fuel loading is needed to allow for fuel burnup. During 2-year operation at a power level of 20,000 kilowatts, approximately 85 kilograms of uranium-235 will be consumed. Some unpublished NASA Fermi age criticality calculations for thermal reactors indicate that by use of burnable poisons an initial fuel loading of three or four times the clean critical loading and a burnup of 50 or 60 percent seems attainable. However, the reactor considered herein will be epithermal or intermediate after loading with extra fuel, and there is no simple way to determine how much can be gained by using burnable poisons in such a reactor. Therefore, a loading of 75 kilograms of uranium-235 and a burnup of 55 percent simply was assumed to be possible for this reactor. With this initial loading and burnup the reactor must be reloaded only once.

Fuel assemblies. - The only fuel considered in this study is uranium-235. Since metallic uranium will melt at the reactor operating temperatures, the fuel will have to be in high-temperature-resistant compounds such as uranium oxide UO_2 or uranium carbide UC_2. The oxide has a very high melting point and its technology is well known, but uranium carbide, which also has a high melting point, has a better heat conductivity and might be preferable. Uranium carbide was chosen for this study, but if uranium oxide had been selected, the results would not be substantially different.

The reactor is loaded with uranium-235 fuel enriched to 93.5 percent. The fuel, in the form of uranium carbide is incorporated into flat-plate-type fuel assemblies. The rectangular fuel plates consist essentially of uranium carbide particles uniformly dispersed and imbedded in molybdenum along with a small amount of poison, and the fuel is clad on each side with molybdenum. The thickness of the fuel plate is 0.031 inch.

The fuel plates are contained in a fuel assembly, which is 3.1 inches on a side and 30 inches long. The fuel assembly structure consists of two molybdenum side plates, 0.050 inch thick, and a molybdenum center support plate, 0.025 inch thick. There are a total of 28 fuel assemblies in the reactor. Each fuel assembly contains 21 fuel plates with a nominal spacing of 0.12 inch between each plate. The fuel assemblies are placed in molybdenum sleeves in the beryllium oxide moderator in order to contain the liquid sodium coolant. The sleeve thickness is 0.050 inch on a side.

Reactor weights. - The total reactor weight is 4070 pounds; the breakdown is as follows: reactor core, excluding fuel elements and coolant, 1450 pounds; fuel elements for one loading, 800 pounds; reflector, 1600 pounds; and sodium coolant in the core, 220 pounds.

HEAT-EXCHANGER DESIGN

A heat exchanger is used to transfer heat from the radioactive liquid sodium in the primary loop to the nonradioactive sodium in the secondary loop. The shell and tube heat exchanger assumed for this analysis is a U-bend fixed-tube-sheet exchanger made of molybdenum. Further, it is assumed that the tubes are in a triangular pattern with a 0.40 inch pitch; the tube inside diameter is 0.25 inch; the sodium velocity in the tubes is 30 feet per second.

The basic equations used to design a heat exchanger for this analysis are given in appendix C along with a sample calculation for an electric power output of 20,000 kilowatts. No attempt was made to optimize the performance or weight of the equipment. A summary of heat-exchanger data is given in table I for the assumptions stated previously.

SHIELDING ANALYSIS

The space-vehicle configuration chosen for this application, described previously, is shown in figure 1. In order to calculate the shielding required to protect the crew, an outer diameter of 80 feet was selected for the crew compartment. This diameter, has the following qualities: (1) there is no large variation in body forces in the crew compartment, (2) this diameter provides a body force of approximately 1 g at a reasonable rotative speed, and (3) it is compatible with the other components of the space vehicle, particularly the radiator.

The radiator was placed between the reactor and crew compartment to minimize the amount of structure required. It was tapered, as shown in figure 1, in order to stay within the solid angle defined by the

reactor and crew compartment. This arrangement would also permit an approach to the crew compartment by another vehicle even after the reactor and radiator are put into service.

In the present study, shielding of the crew from the reactor radiation only was considered. The radiation shielding geometry consists of a neutron shield between the reactor and heat exchanger, and a gamma shield between the heat exchanger and the crew compartment (fig. 8). The neutron shield prevents the sodium working fluid from becoming activated, and also serves as a gamma shield. The gamma shield serves to shield from gamma activity originating from both the reactor and the primary sodium. In addition, gamma shielding from the reactor is provided by the sodium in the heat exchangers, headers, and piping. Because air scattering is absent in space applications, shadow shielding is sufficient for both the neutron and gamma shields.

Shield Materials

The use of high-temperature shield materials is required in this application because of the high temperatures (up to 2800° R) encountered in the reactor and heat exchanger. For this reason, boron carbide B_4C was chosen for the neutron-shield material and tungsten was chosen for the gamma-shield material. In addition, a heavy metal hydride was considered for the neutron shield for comparison purposes only. Although the shield material problem was not investigated in great detail, it is believed that the choice of boron carbide and tungsten were reasonable because both materials have the desired thermal and nuclear properties.

Neutron shield. - Boron carbide has good neutron slowing down and absorption properties in addition to its high melting point. The nuclear properties of naturally occurring boron were used in determining the required neutron-shield thickness.

Boron carbide has two other attractive features for use as a neutron shield. One of these features is that only a relatively few soft capture gammas are given off. The other feature is that the gamma rays arising from neutron inelastic scattering are not a serious problem.

Gamma shield. - Tungsten is a good gamma-shield material for this application because it has both a high density and high melting point. The reduction of the gamma radiations from a point source is accomplished almost entirely by the thickness density (gm/cm^2) of material between the source and detector. For a spherical shield, therefore, the shield weight is reduced by using a high-density material. This same principle applies to the present shield configuration and thus it was desirable to use not only a high-temperature material but one of high density as well.

The tungsten shield was used in order to protect from both the primary sodium gamma activity and the reactor activity. In all of the cases investigated, the gamma-shield thickness was determined by the primary sodium activity.

Calculation Procedure

In calculating the shield dimensions it was necessary to make a number of abbreviating assumptions in order to obtain answers within a reasonable length of time. References 7 to 10 were the sources of information drawn upon for most of the assumptions and methods of calculating shield dimensions. Only the main assumptions and principle procedures followed will be presented here in outline form.

An exponential attenuation in conjunction with a linear buildup factor was assumed for both the neutron- and gamma-attenuation calculations. For neutron attenuations the linear buildup factor (ratio of shield thickness to relaxation length) was taken to be the ratio of the boron carbide thickness to a relaxation length obtained by taking the reciprocal of the removal cross section given in reference 9 for boron carbide. Although it is not theoretically correct to use the removal cross section in this manner, the error incurred is consonant with the accuracy of the over-all calculation procedure. The buildup factor for gamma attenuation was taken as the ratio of tungsten thickness to the relaxation length of 4 Mev gamma rays in tungsten.

The reactor was treated as a cylindrical source with uniform power per unit volume. All gamma rays and neutrons emanating from the reactor were taken to have an energy of 4 and 8 Mev, respectively (ref. 7). It was also assumed that 20 Mev of energy in the form of gamma energy were released per fission (ref. 7). The intensity of the fast neutron and gamma flux in the reactor was determined from the equations on page 34 of reference 8. Gamma radiation resulting from inelastic neutron scattering was neglected. These gamma rays were ignored when it became apparent that the tungsten-shield thickness was determined by the primary sodium activity.

Calculations of the shielding required for the primary sodium activity were made assuming the activity stemmed from a uniformly distributed cylindrical source the size of the heat exchanger. The accepted decay scheme and thermal neutron cross section of sodium was used in determining its activity. In calculating the shield thickness, the absorption coefficient for 4 Mev gamma rays was used as in the case of the reactor shielding. This results in a conservative answer since the sodium gammas are not this energetic. The primary sodium activity was assumed to be constant because the reactor time of operation was long enough and

the decay constant for the sodium was large enough that the sodium attained secular equilibrium (i.e., the activity becomes constant with time).

A simple distance attenuation between the shield-face dose and crew dose was assumed. Scattering from the radiator or other spaceship structure was ignored and none of the structure, equipment, and so forth was credited as shield material. All machinery, radiator, structure, and so forth, were positioned within the solid angle prescribed by the crew compartment and reactor. The crew dose rate allowed was 100 mrem per week.

To completely eliminate the activation of the secondary sodium by the neutron flux from the reactor would be impractical if not impossible. For this reason a secondary sodium activity was permitted, which would give the crew a dose equal to 0.01 of the total allowable. The assumptions made in calculating this allowable activity (and, thus, allowable heat-exchanger flux) were that: (1) For dose calculation purposes the secondary sodium activity was considered to be concentrated as a point source on the axis of rotation midway between the shield face and the face of the crew compartment, (2) the crew dose received from this activity was attenuated simply by the distance between the crew and source of radiation, and (3) the sodium attained secular equilibrium.

Shield weights were calculated for two separation distances, which were selected as the minimum distance that would permit placing the radiator between the shield and crew quarters, and the maximum separation distance that appeared practical. Separation distances of 286 and 624 feet were used; these particular numbers are the result of a trial-and-error procedure used in the shield calculations. For a distance of 286 feet the total shield weight (neutron plus gamma shields) was 38,000 pounds. This weight decreased to 24,500 pounds for a separation distance of 624 feet. The combined weight of the shield, piping, and structure for the 624-foot distance was about 8000 pounds less than that for the 286-foot distance. Thus, the space vehicle configuration having a separation distance of 624 feet was selected for this report.

No provisions were made in the shielding calculations for the sodium piping. In order to shield against the gamma rays given off by the primary sodium piping, the tungsten-shield dimensions were increased (fig. 8). To shield the secondary sodium piping from the reactor neutron flux, one boron carbide shield dimension was also increased. Because the shield materials were selected to withstand very high temperatures, the shield cooling problems are greatly simplified. It was assumed that if thermal radiation from the shield was not sufficient to take care of the gamma heating, the required cooling could be obtained by using the primary sodium as a coolant. In addition, the use of a shadow shield and its near weightlessness in space would make it possible to design a practically restraint-free shield and thus mitigate the thermal-stress problem.

In comparing boron carbide with the heavy metal hydride as neutron-shield material, it was found that the heavy metal hydride resulted in a thinner shield but its weight was approximately 2.7 times the boron carbide shield weight. The reduction in neutron-shield thickness using the heavy metal hydride made a savings in the tungsten gamma-shield weight possible. However, this reduction in weight was quite small and did not offset the added neutron-shield weight. The total weight, therefore, of the neutron plus gamma shield was greater (approximately 60 percent) when the heavy metal hydride was employed. It should be noted that for other shield configurations (e.g., a unit shield), the use of a heavy metal hydride could yield a lighter shield. (The shield weights arrived at for this space vehicle are probably conservative.)

Cosmic Ray Radiation

The amount of cosmic ray radiation in space and the effects on humans are two of the unknowns that could exert a profound influence on space-vehicle design. Experimental measurements will probably establish in the not too-distant future the composition and distribution of cosmic radiations in space. The effects on humans of this cosmic radiation will not be established quite so readily. These effects must be determined, however, before a truly rational space-vehicle design can be undertaken.

Recent artificial earth satellite data have shown intense low-energy radiation existing in space that increases in intensity with distance from the earth. These new discoveries increase what was already a potentially hazardous condition. Dr. Schaefer in his many papers (ref. 11) estimated that the dose received from cosmic radiation known prior to the satellite data could be very high. This dose, which was over 100 mrem per day in space, was obtained by extrapolating known radiation ionization effects to those resulting from cosmic rays. It should be noted, however, that others working in this field had not felt that cosmic radiations constituted a serious problem but in most instances they had not viewed the problem on a long-time-exposure basis. In any event, it is universally agreed that very thick shields will be required if the high-energy particles involved in Dr. Schaefer's calculations are to be stopped by conventional shielding techniques. Very few calculations or measurements of the amount of shielding required for protection from these cosmic rays have been made. However, a simplified calculation for continuous exposure indicates that the order of magnitude for these shield thicknesses will probably be 12 or more inches of aluminum. In such an event, the reactor shielding will be viewed entirely differently as will the crew compartment management. It might also be noted that this amount of shielding will probably prove adequate for protection from the low-energy radiations disclosed by the satellites.

CONDENSER RADIATOR

General Configuration

The heat-rejection system of the space-vehicle powerplant involves two primary functions: the condensing of the discharge vapor and the rejection of its latent heat through radiation into space. Vapor condensation may present a problem in such a space system because of the absence of net body force. However, condensate removal can be enhanced either by centrifugal force through rotation of the condensing surfaces or by mechanical means, such as the action of wiper blades. The design of a suitable heat-rejection system was therefore governed by consideration of both total weight and of simplicity and effectiveness of the condensate-removal system.

In general, two arrangements are possible for the heat-rejection system: separate condensing and radiating units with a secondary cooling system between them can be used or both functions can be combined into one component. In the single-component system, the vapor of the mixture discharged from the turbine is condensed at constant temperature on the inner surfaces of flow passages that consist of tubes or channels. The latent heat of condensation is conducted across the walls of the flow passages and is then radiated into space from the outer surfaces. Condensate removal is facilitated by rotation of the passages to provide a centrifugal force in the direction of the flow.

In the separate-component system, vapor is condensed on the surface of the condenser unit, and the condensate is collected (by rotation or mechanical means) and returned to the cycle. The heat of condensation is absorbed by a liquid coolant circulating between the condensing surfaces and the separate radiator unit. The separate-unit system has an advantage in that smaller and lighter radiator piping is required because of the smaller volume flow rates than in the vapor radiator. However, this weight reduction will be counteracted by the additional weight of the separate condenser and of the greater radiating surface area required by the liquid radiator. A larger radiating surface is required by the separate radiator compared with the integral vapor radiator because the average surface temperature of the liquid radiator will be lower than the surface temperature of the condensing vapor radiator.[1] A lower total weight for the separate component system therefore appears highly unlikely. As a consequence and in the interests of simplicity, it was decided to use a single condenser radiator that combines both functions.

---

[1]A lower average surface temperature occurs for the all-liquid radiator because a temperature drop will exist along the flow in the radiator and also because the maximum liquid temperature in the cooling loop will be lower than the temperature of the vapor in the condenser.

The general configuration of the condenser-radiator was governed by the primary requirements (1) that it be contained within the cone angle of the protected volume behind the shield and (2) that it be sufficiently removed from the crew compartment in order to minimize the heat transfer to the compartment. The radiator was consequently located approximately 220 feet from the reactor with a maximum radial length (or length normal to the axis of the vehicle) at the front end of approximately 16 feet (fig. 1). The radiator is thus forced into a configuration of comparatively long axial length and short radial height.

In selecting the general geometric form of the radiating surface, two possibilities were considered; a truncated surface of revolution rotating about its axis, and a plane of trapezoidal plan form rotating about the long axis through its center of gravity. For this vehicle, only one side of the surface of revolution can be used to radiate heat, and thus, for a given wall thickness the surface of revolution will be considerably heavier than the plane in which both surfaces can be utilized. It appeared more desirable therefore to adopt the trapezoidal plane as the geometric form for the radiator.

The primary radiator structure was designed as a series of individual constant cross-section tubes laid side by side. This type of construction has the advantage of simplicity of fabrication and assembly, as well as of analysis.[2] In order to allow for the contingency of tube puncture due to meteoroid impact, it may be necessary to close off the flow in each tube (tube diameters are sufficiently large, 3.3 to 5.25 in., to permit such a scheme), or even effect repairs of individual tubes.

As a further precaution against the loss of vital fluid in the event of malfunction of the individual tube shutoff valves, the radiator was divided into eight independent sections of equal surface area. Each tube section has inlet and outlet headers and valves so that the section can be cut off from the main flow.

A schematic diagram of the general radiator construction is shown in figure 9. Vapor from the turbine flows along the central delivery pipe (on the axis of rotation) and enters the individual section headers through the connecting pipes. The vapor is then distributed to the individual tubes where it is condensed (latent heat is radiated from the tube outer surface). The condensate is centrifuged into the outlet

---

[2]A sandwich-type construction consisting of two separated flat plates was also considered in which the necessary supporting structure in between the plates forms the flow passages. However, a rough calculation showed that for the same stress, the sandwich construction tends to give a greater weight than the tube construction.

headers and thence into the outer return pipes and is collected in the pump well at the outermost periphery of each segment. The pumps then drive the condensate through the central return pipe. Cutoff valves are located in the short connecting pipes at the inlet and outlet headers of each tube section. A suitable supporting structure is used to reinforce the various components of the radiator.

Design Values

The principal design factors governing the weight of the radiator for a given radiating surface area were found to be the density of the material used for the structure, the wall thickness of the radiating tubes and of the supply piping, and the velocities of the fluid in the various components of the radiator. Principal attention in the design was therefore directed to these factors.

Material. - A desirable material for radiator application is one with adequate creep strength at the operating temperature (1340° F) and pressure (2.7 lb/sq in.) of the unit, good resistance to corrosion with sodium, good meteoroid-impact resistance, and low density. Stainless steel was selected as a satisfactory material for the radiator. Type 304 or type 316 stainless steel, for example, is expected to have a creep strength of over 2000 pounds per square inch for 2 percent creep in 20,000 hours at 1340° F, while the combined tube stresses due to internal pressure and centrifugal force were computed to be of the order of 400 pounds per square inch. (Beryllium appears to have properties superior to those of stainless steel for radiator application; but beryllium was not specified in the design because of the uncertainty in its feasibility of fabrication and high-temperature properties.)

Wall thickness. - Because of the comparatively low fluid pressures in the system, operating stress was not a significant consideration in the selection of the tube and pipe wall thickness. The principal concern was for penetration damage incurred by impact with meteoritic particles. In general, the probable number of penetrations that can be allowed in a component will depend on the resultant damage to or disruption of operation of the unit. For the radiating tubes, if a puncture is sustained, the tube can be shut off permanently. The loss in radiating surface area in such cases can be compensated by the surplus radiating area contained in the inlet piping and headers and also by a possible gradual increase in the emissivity of tube surfaces due to meteoritic erosion. Thus, it may be reasonable to allow for tube loss of 10 to 20 percent due to meteoritic action. For the delivery and return piping, however, it is essential to design for an extremely low puncture probability, since such an occurrence might be catastrophic for the unit.

Unfortunately, reliable estimates of meteoritic puncture probability cannot be made currently. The radiating tube wall thickness was consequently arbitrarily selected as 0.025 inch. For this wall thickness, according to the meteoroid hit frequency data and the proposed penetration criterion of Whipple (ref. 12), approximately 15,000 penetrations might be sustained during the lifetime of the vehicle. However, extrapolation of existing experimental data on cratering effects in high-velocity particle impact (e.g., refs. 13 and 14), after suitable correction for the difference between meteoroid and tube material density, indicates that only about two or less penetrations might be expected during the lifetime of the vehicle.

For the radiator supply piping, the wall thickness was increased to 0.125 inch in order to provide a substantial resistance to penetration. In addition, all supply pipes were enclosed within a 0.025-inch-thick steel meteor bumper (ref. 15) located a distance above the outer surface of the pipe equal to about 0.1 the diameter of the pipe. The bumpers are calculated to sustain between 2800 to less than one penetration during the lifetime of the vehicle. However, the meteoroids possessing sufficient energy to pierce the wall of the bumper will be fragmented into many smaller particles before they impinge on the surfaces of the pipes. The probability of a puncture of the piping walls will therefore be quite small.

Flow velocity. - In general, it is desirable to maintain fluid flow velocities throughout the radiator as high as possible so that pipe size and, therefore, weight can be reduced. However, velocity limitations may be incurred in the various components because of considerations of excessive friction pressure drop, possible choked flow, and excessive corrosion rates. Values of flow velocity selected for the various components are listed in the following table:

Component	Velocity, ft/sec	Remarks
Central delivery pipe (vapor)	1285 (M = 0.6)	Choke limit.
Inlet headers (vapor)	1088 (M = 0.5)	Choke limit.
Radiating tubes (vapor)	100	Total tube weight independent of tube size. Low velocity to give large tube diameter and small difference between vapor stagnation and static temperatures
Return headers and pipe (liquid)	4	Friction drop must be less than pressure rise resulting from centrifugal force
Return pipe downstream of pump (liquid)	20	Corrosion limit.

The total radiating tube weight is independent of tube size because the product of tube diameter and number of tubes is constant for a given required radiating surface area (appendix D). A small difference between radiating-tube stagnation and static temperature is desired so that the radiating surface temperature, which depends on vapor static temperature, can be maintained as high as possible. In the outlet headers, it is desirable to have a net pressure rise so as to favor the avoidance of cavitation difficulties in the pump (condensate will closely approach saturated state).

Pumps

Each condensate pump at the outer periphery of the radiator is required to deliver 248 gallons per minute at a head of about 100 feet. If an electromagnetic pump is considered with an efficiency of approximately 35 percent, the power required for each is 13.6 horsepower and, according to the limited data of reference 16 (p. 347), a weight of approximately 175 pounds might be expected.

Heat Transfer

Inasmuch as required radiant surface area (and, therefore, radiator weight) varies inversely with the fourth power of the temperature of the radiator outer surface, it is desirable to effect as small a temperature drop as possible between the fluid bulk inside the tubes and the tube outer surfaces. According to the heat-transfer equations in appendix D, the magnitude of the condensing heat-transfer coefficient will largely determine the temperature drop, and large values of this coefficient are desired. In the absence of data on condensing heat-transfer coefficients for liquid sodium, a temperature difference of 20° F between the turbine-outlet total temperature and the radiator surface temperature was assumed for the cycle calculations. This temperature difference requires a condensing heat-transfer coefficient of approximately 685 Btu per hour per square foot per $^{\circ}$ F. It is believed that the rotative speed of the radiator (which produces a maximum acceleration of 3/4 g) is sufficient to maintain the heat transfer within the specified temperature difference.

For the radiant heat transfer from the radiating tubes, it was assumed that the emissivity can be maintained approximately at a value of 0.90 (either through the use of special coatings or the erosive action of micrometeoritic particles), and that the effective radiating area of the tube surfaces is equal to the projected area of the tubes. That is,

$$A_n = 2\bar{l}_n N_n d_{o,n} \tag{13}$$

Stresses and Structure

In order to reduce the weight of required accessory structure, the radiating tubes and outlet headers and pipes can be allowed to be self-supporting, with the centrifugal load transmitted by the tubes to the inlet headers. No difficulty is anticipated with this arrangement, inasmuch as the total centrifugal stress at the base of the radiating tubes (at inlet header) was computed to be of the order of 50 pounds per square inch for stainless steel at a rotative speed of 7.6 rpm. The supporting structure can then be restricted to a frame connecting the two inlet headers (the frame will have to carry a direct centrifugal load of approximately 5000 lb) and possibly also to a connecting support for the pumps at the outer periphery. The weight of the supporting structure can probably be limited to approximately 2000 pounds.

Total Weight

The total weight of the condenser-radiator is summarized as follows (the various equations used to compute component weight are derived in appendix D):

Component	Weight, lb
Radiating tubes	23,220
Central delivery pipe	8,320
Inlet and outlet headers and connecting pipes	6,010
Return pipes	2,810
Pumps	350
Sodium	1,240
Structure	2,000
Total	43,990

In view of the many assumptions and speculations involved in the analysis, the foregoing results should be regarded as a rough evaluation of the condenser-radiator function. No attempt has been made to optimize the design within the limits of the imposed specifications, and it is also recognized that other schemes or geometric configurations are possible for the application. However, the present analysis indicates the weight levels and design problems that might be expected for such a unit.

TURBINE DESIGN

For the selected powerplant design conditions, the required turbine work is 357 Btu per pound and the turbine total-pressure ratio is 25.

For the selected turbine-design conditions of saturated vapor at the turbine inlet, the equilibrium state of the working fluid at the turbine exit corresponds to a liquid content of 21 percent (exit quality, 0.79). Knowledge of whether such a condition is tolerable or whether erosion of the turbine blades results from this condition will require operating experience with a turbine and working conditions similar to those considered herein. Reference 17 indicates that superheating is not required for commercial mercury-vapor turbines having exit qualities of 0.85 or 0.86. Whether or not the high gas velocities of the high-performance turbine considered herein would alleviate or aggravate the erosion problem is not clear. If liquid droplets form, the high speeds of the droplets relative to the turbine blades will probably increase erosion. On the other hand, the short time that the working fluid resides within the turbine may result in the nonequilibrium condition of supersaturation without any droplet formation until the vapor leaves the turbine; this lack of equilibrium probably also will decrease the turbine efficiency.

The selected turbine is an axial-flow type having four stages. The combination of blade stress and temperature is most severely limiting in the first rotor blade row, and the rotational speed was selected on this basis. For a power output of 20,000 kilowatts, the turbine-tip diameter is 64 inches, and the weight is estimated to be 10,500 pounds.

The method by which the turbine was selected is described in appendix E.

GENERATOR DESIGN

Generator weight was estimated by extrapolation of the weights of two small commercially-available aircraft generators. These generators have the following characteristics: (This information was obtained from Mr. James Hibbard, Jack & Heintz, Inc., Cleveland, Ohio)

Output, kva	Weight, lb
10	20
200	250

The power factor of generators for use in this analysis was considered to be 1.0. Departure of power factor from 1.0 would result in a penalty in generator weight inasmuch as, for generators limited by cooling capacity, the specific weight would vary inversely with the power factor.

From the preceding data, the following equation was written

$$\frac{W_g}{\text{Power output}} = 2.87(\text{Power output})^{-0.157} \qquad (14)$$

(The form of eq. (14) is quite arbitrary.) At the 20,000-kilowatt level, generator specific weight from this relation is 0.6 pound per kilowatt.

Generator cooling in space is a problem because the waste heat must be rejected by thermal radiation. Even a generator having an efficiency of 0.95 must reject a megawatt of heat in order to produce 20,000 kilowatts of electric power. In order for the radiator that rejects this heat to be small, the radiator must be hot. This requires either (1) high-temperature operation of the generator, or (2) use of a refrigeration system that permits operating the radiator at a temperature higher than that of the generator. The refrigerating system was not analyzed. Instead, the generator was considered to operate at a temperature of 1200° R and to be maintained at this temperature by circulation of terphenyl vapor. A portion of the circulating terphenyl vapor was considered to be bled from the generator-cooling loop, condensed in a radiator, and sprayed into the recirculating stream of vapor that cools the generator. The estimated weight of the radiator necessary for cooling the generator was 2500 pounds. No detailed analysis of this radiator was made.

SEPARATOR-EVAPORATOR DESIGN

Instead of boiling in the intermediate heat exchanger, a separator-evaporator was included in the system (fig. 8). In this evaporator the liquid is expanded from point 5 to point 6 on figure 6 and the resulting vapor separated from the liquid as described in CYCLE CONSIDERATIONS. Rotation of the fluid and its concomitant centripetal acceleration provide the buoyant forces required for separation.

The pressure drop from 200 pounds per square inch at the heat-exchanger exit to 69 pounds per square inch at the turbine inlet was used to obtain high rotational speed within the evaporator. An evaporator filled with liquid but having a 1-foot-diameter cylinderical "hole" of vapor in the middle would, for the specified pressures, have a centripetal acceleration of about 1800 g at the surface of the liquid. Such a high acceleration should permit adequate separation of the two phases.

For the 20,000-kilowatt system, the evaporator weight was estimated as follows: The evaporator shell was considered to be spherical and to have its wall thickness determined by the stress required to avoid rupture in 100,000 hours at 2500° R and with an internal pressure of 200 pounds per square inch. The resulting shell weight is 135 pounds. The sphere was considered to be half filled with liquid sodium, giving a total weight of 434 pounds.

POWERPLANT SUMMARY

A design summary of the nuclear turboelectric powerplant considered in this study is given in table II, and a system weight breakdown is given in table III. The total powerplant weight was calculated to be about 6 pounds per kilowatt for 20,000 kilowatts of electric power output. The radiator contributes about 2.1 pounds per kilowatt to the total weight and the reactor and reactor shield contribute about 0.24 and 1.2 pounds per kilowatt, respectively. The generator, turbine, and piping make significant contributions to the total weight (between 0.5 and 0.6 pound per kilowatt), while the heat exchanger, pumps, etc. are less important. It is significant that the radiator has the dominant weight in spite of the fact that the powerplant design was varied in order to minimize this weight.

As the design value of power is decreased, it is expected that the weight per kilowatt of most of the items listed in table III remains essentially constant. The shield is an obvious exception. As the design power changes, shield weight changes slowly, with the result that its weight per kilowatt climbs steeply as power decreases.

CONCLUDING REMARKS

This study has been directed toward exploring the design of a nuclear turboelectric powerplant suitable for a manned space vehicle with interplanetary capability. The study was concentrated on a powerplant with an electrical power output of 20,000 kilowatts, and the specific conclusions for powerplants of this size or larger are as follows:

(1) The radiator has the dominant weight and the powerplant operating conditions should be selected to reduce radiator weight.

(2) The minimum radiator area, for a fixed turbine-inlet temperature, occurs at a relatively fixed value of the ratio of radiator-inlet to turbine-inlet temperature (approximately 0.75). The turbine-inlet temperature should be as high as possible in order to maximize radiator-inlet temperature and therefore minimize radiator area.

(3) The working fluid for the thermodynamic cycle should probably be a liquid that is boiled and condensed. If the working fluid is a gas, the turbine-inlet temperature would have to be about 1.6 to 1.8 times as great in order for the radiator area to be as small as for a vapor cycle.

(4) The radiator should be designed to reduce, limit, and perhaps permit meteoroid-damage repair.

(5) Reactor weight is a comparatively small part of total powerplant weight, and a large amount of fuel will be consumed during powerplant operation. From general considerations, it can be seen that at lower power levels (approximately 100 kw), the reactor weight is a large part of total powerplant weight, and smaller amounts of fuel will be consumed.

(6) The shield weight is an appreciable part of the total powerplant weight (approximately 20 percent), but it is not dominant as it would be at lower power levels.

The results of this study have established several important research areas associated with the development of a reliable nuclear turboelectric powerplant of the type described herein. These research areas fall into three main categories, as follows:

(1) Energy source:

(a) Design and control of compact reactors for continuous and reliable operation at high temperatures for 1 or 2 years

(b) Adequate methods of calculating shadow shields at temperatures so high that hydrogenous materials may not be suitable

(2) Energy conversion systems:

(a) Design of components such as metallic-vapor turbines and high-performance generators for lengthy reliable operation

(b) Corrosion by metallic liquid and vapor for new ranges of operating conditions and new materials

(c) Thermodynamic property evaluation of liquefied and vaporized metals at higher temperatures than are currently available

(d) Heat transfer upon boiling and condensing of liquid metals under zero gravity conditions

(e) Strength of materials and radiation damage at high temperatures for extended periods of time

(3) Space environment:

(a) Meteoroid damage and methods of protection from meteoroids

(b) Shielding for human protection against cosmic radiation

Each of the three main research areas listed previously overlaps the others, and the solutions found in any given area will aid in the solution of problems in the remaining areas.

Lewis Research Center
National Aeronautics and Space Administration
Cleveland, Ohio, November 26, 1958

E-156

CO-4 back

APPENDIX A

SYMBOLS

The following symbols are used in this report. Consistent units are used:

A	effective radiant surface area
A_f	flow area
a	over-all length of radiator
B	width of fuel plate
b	length of radiator delivery pipe
C	vapor velocity of sound
c_p	specific heat at constant pressure
D	diameter
D_R	reactor diameter
d	tube or pipe inside diameter
d_e	equivalent diameter
d_o	tube or pipe outside diameter
F_a^*	ratio of maximum to average rate of power generation axially
f	friction factor
g	standard gravitational acceleration
H	specific enthalpy
H_c	heat of condensation
h	heat-transfer coefficient
J	mechanical equivalent of heat
k	thermal conductivity
L	distance from center of rotation of radiator

L_R	reactor length
l	length of tube or pipe
M	Mach number
m	average molecular weight
N	number of tubes
Nu	Nusselt number, hd_e/k
P	power input or output
P_{re}	reduced vapor pressure
Pr	Prandtl number, $c_p\mu/k$
p	pressure
Q	heat-transfer rate
q	heat-transfer rate per unit surface area
R	radius of heat-exchanger tube bundle
$\overline{R}$	universal gas constant
Re	Reynolds number, $\rho V d_e/\mu$
S	specific entropy
S_h	heat-transfer surface area
T	temperature
T_{re}	reduced temperature
$(\Delta T)_{ln}$	log mean temperature difference
t	wall thickness of tube or pipe
U_o	over-all coefficient of heat transfer based on outside surface
U_h	blade velocity at turbine hub
V	velocity
v	volume

W	weight
w	weight-flow rate
X	quality of vapor (fraction in vapor phase)
α	ratio of reactor flow area to reactor core cross-sectional area
β	half cone angle of shield
Γ	stress
γ	ratio of specific heats
ϵ	emissivity
η	efficiency
η_g	product of generator and mechanical efficiency
θ	maximum temperature difference between reactor coolant passage surface temperature and coolant temperature
λ	tube pitch
μ	absolute viscosity
ρ	density
σ	Stefan-Boltzmann constant for radiation
Ω	rotational speed
ω	defined by equation (B14)

Subscripts:

C	compressor
cr	critical
d	delivery pipe
e	electric
g	generator
h	header

i	ideal or isentropic
j	integer corresponding to individual radiating tube
l	liquid
m	material
n	integer corresponding to tube section
o	outside surface
R	reactor
r	radiating
re	reduced
s	saturated vapor
T	turbine
t	tubes
v	vapor
w	wall
1	start of compression process (radiator exit)
2	start of heat addition process
2'	start of boiling process
3	start of expansion process (turbine inlet)
4	start of heat rejection process (radiator inlet, turbine exit)
α	primary sodium entering heat exchanger
β	primary sodium leaving heat exchanger
γ	secondary sodium entering heat exchanger
δ	secondary sodium leaving exchanger

Exponents:

n	polytropic constant

APPENDIX B

EQUATIONS FOR RATIO OF RADIATOR AREA TO ELECTRIC POWER OUTPUT

Gas Cycle

The heat rejected by the system is radiated to space. Consider the radiator to be a tube with the gas entering at temperature T_4 and leaving at temperature T_1. Assume that the radiator wall temperature is equal to the gas temperature in the tube, and that the sink temperature is 0° R. Then, for an element of radiator surface area, dA, the following may be written:

$$-wc_p dT = qdA = \sigma\epsilon T^4 dA \tag{B1}$$

Integration of equation (B1) between the temperature limits of T_4 to T_1, results in the following equation after some simplification

$$wc_p(T_4 - T_1) = 3\sigma\epsilon A \frac{T_4^3 T_1^3}{T_4^2 + T_1 T_4 + T_1^2} \tag{B2}$$

which may be written as

$$wc_p T_3\left(\frac{T_4}{T_3} - \frac{T_1}{T_3}\right) = 3\sigma\epsilon A T_3^4 \frac{\left(\frac{T_1}{T_3}\right)^3\left(\frac{T_4}{T_3}\right)^3}{\left(\frac{T_4}{T_3}\right)^2 + \left(\frac{T_1}{T_3}\right)\left(\frac{T_4}{T_3}\right) + \left(\frac{T_1}{T_3}\right)^2} \tag{B3}$$

The net power output is given by

$$P_{net} = P_T - P_C \tag{B4}$$

or in terms of electric power output,

$$P_e = (2.93\times10^{-4},\ \text{kw/(Btu)(hr)})\eta_g P_{net} \tag{B5}$$

where

$$P_T = wc_p(T_3 - T_4) = w\eta_T c_p T_3\left[1 - \left(\frac{p_4}{p_3}\right)^{\frac{\gamma-1}{\gamma}}\right] \tag{B6}$$

and

$$P_C = wc_p(T_2 - T_1) = \frac{wc_pT_1}{\eta_C}\left[\left(\frac{p_2}{p_1}\right)^{\frac{\gamma-1}{\gamma}} - 1\right] \tag{B7}$$

Combining and simplifying equations (B3) to (B7) yields

$$\frac{A}{P_e}\left(\frac{\text{sq ft}}{\text{kw}}\right) = \frac{\left(\frac{T_4}{T_3} - \frac{T_1}{T_3}\right)\left[\left(\frac{T_4}{T_3}\right)^2 + \frac{T_1}{T_3}\frac{T_4}{T_3} + \left(\frac{T_1}{T_3}\right)^2\right]}{1.53\epsilon\eta_g\left(\frac{T_3}{1000}\right)^4\left(\frac{T_1}{T_3}\right)^3\left(\frac{T_4}{T_3}\right)^3\left\{\left(1 - \frac{T_4}{T_3}\right) - \frac{T_1}{T_3}\frac{1}{\eta_C}\left[\frac{\left(\frac{p_2}{p_3}\frac{p_4}{p_1}\right)^{\frac{\gamma-1}{\gamma}}}{1 - \frac{1}{\eta_T}\left(1 - \frac{T_4}{T_3}\right)} - 1\right]\right\}} \tag{1}$$

E-156

Vapor Cycle

CO-5

For the vapor-cycle analysis, the pressure ratios $p_{2'}/p_2$ and p_4/p_1 (fig. 2) were taken equal to 1.0. The pump work required to maintain these pressures as well as the work required to pump the liquid from point 1 to 2 (fig. 2) is negligible. The net power output is

$$P_{net} = w(H_3 - H_4) \tag{B8}$$

where the actual enthalpy at point 4 H_4 is related to the ideal enthalpy $H_{4,i}$ through the turbine adiabatic efficiency η_T by

$$(H_3 - H_4) = \eta_T(H_3 - H_{4,i}) \tag{B9}$$

In terms of electrical power output, equation (B8) becomes

$$P_e = 2.93\times10^{-4}\eta_g w(H_3 - H_4) \tag{B10}$$

Now, heat is rejected in the radiator at a constant temperature (condensing vapor) by radiation to space. For a sink temperature of 0° R, and assuming that the radiator surface temperature is equal to T_4, the following heat balance for the heat rejection is

$$w(H_4 - H_1) = \epsilon\sigma AT_4^4 \tag{B11}$$

or

$$A = \frac{w(H_4 - H_1)}{1.73\times10^{-3}\epsilon\left(\frac{T_4}{1000}\right)^4} \tag{B12}$$

The ratio of radiator area to electric power output from equations (B10) and (B12) is then

$$\frac{A}{P_e}\left(\frac{\text{sq ft}}{\text{kw}}\right) = \frac{1.972\left(\frac{H_4 - H_1}{H_3 - H_4}\right)}{\epsilon\eta_g\left(\frac{T_4}{1000}\right)^4} \tag{2}$$

Equation (2) was used to obtain the mercury and sodium curves shown in figure 5. The thermodynamic properties of sodium were obtained from reference 18. No thermodynamic properties of mercury were available above a temperature of 1860° R (ref. 19). Consequently, the following method was used to extend the mercury properties of reference 19 up to a temperature of 3000° R.

According to reference 20, the entropy of vaporization is given by

$$\Delta S = \Delta S^{(0)} + \omega\,\Delta S^{(1)} + \omega^2\Delta S^{(2)} \tag{B13}$$

where the acentric factor ω is defined as

$$\omega = -\log_{10}P_{re} - 1.00) \tag{B14}$$

(with P_{re} the reduced vapor pressure, P/P_{cr} is evaluated at the reduced temperature of $T_{re} = T/T_{cr} = 0.70$). The vapor pressure is given by

$$\log P_{re} = (\log P_{re})^0 + \omega\left(\frac{\partial \log P_{re}}{\partial\omega}\right)_T \tag{B15}$$

Values of $-(\log P_{re})^0$, $-(\partial \log P_{re}/\partial\omega)_T$, $\Delta S^{(0)}$, $\Delta S^{(1)}$, and $\Delta S^{(2)}$ are tabulated in table VI of reference 20 for a range of values of T_{re}. Using the tabulated temperatures and pressures of reference 19, a critical temperature T_{cr} of 3125° R and a critical pressure P_{cr} of 15,300 pounds per square inch for mercury (ref. 21), table VI of reference 20, and equation (B15), values of ω were calculated. Since ω is fairly

constant with temperature, an average value was used over the temperature range considered. For this calculation, ω was 0.260.

Equation (B13) was then used to obtain values of ΔS, using a low temperature range that extended into the data of reference 19. At the low temperatures it was found that the values of ΔS determined by equation (B13) were approximately 22.5 percent lower than those of reference 19. Consequently, the values of ΔS obtained by equation (B13) were increased by 22.5 percent.

The entropy of the liquid mercury was determined from

$$S_l = c \ln T/T_o \tag{B16}$$

where

c, the average specific heat of liquid mercury obtained over a temperature range from 490° to 1860° R, is (from ref. 19)

$$c = 0.03154 \text{ Btu/(lb)(°R)}$$

and

$$T_o = 492° \text{ R}$$

The enthalpy of the liquid mercury was obtained from

$$H_l = c(T - T_o) \tag{B17}$$

and the enthalpy change during evaporation is

$$\Delta H = T \Delta S \tag{B18}$$

Thus, using the preceding method, property values of mercury were computed at temperatures above 1860° R.

APPENDIX C

HEAT-EXCHANGER DESIGN FOR A 20,000-KILOWATT ELECTRIC OUTPUT

The heat exchanger is designed to transfer 88,000 kilowatts of heat from radioactive sodium in the primary loop to nonradioactive sodium in the secondary loop. The design is based upon the following previously determined or assumed data:

Primary sodium entering, T_α, $^\circ R$	2800
Primary sodium leaving, T_β, $^\circ R$	2575
Secondary sodium entering, T_γ, $^\circ R$	2475
Secondary sodium leaving, T_δ, $^\circ R$	2700
Total heat to be transferred, Q, Btu/sec	83,350
Sodium weight flow in both loops, w, lb/sec	1235
Sodium velocity in tubes, V, ft/sec	30
Inside diameter of tubes, d, in.	0.25
Tube pitch (triangular pattern), λ, in.	0.40

Properties of Sodium and Molybdenum

The following sodium properties, which are used in these calculations, were obtained by extrapolating the data given in reference 22, for the average temperatures in each loop.

	Primary	Secondary
Temperature, $\overline{T}$, $^\circ R$	2687	2587
Density, ρ, lb/cu ft	44.0	44.0
Absolute viscosity, μ, lb/(hr)(ft)	0.29	0.30
Thermal conductivity, k, Btu/(hr)(ft)($^\circ$F)	28.2	29.0
Specific heat, c_p, Btu/(lb)($^\circ$F)	0.31	0.31
Prandtl number, Pr	0.00319	0.00321

The thermal conductivity, k_m and density ρ_m of molybdenum, the material assumed for the heat exchanger, were obtained from reference 23.

$$k_m = 65 \text{ Btu/(hr)(ft)}(^\circ\text{F})$$

$$\rho_m = 637 \text{ lb/cu ft}$$

An allowable stress of 2500 pounds per square inch was assumed for molybdenum for a rupture life of 20,000 hours. This value was based on data given in reference 24.

Outside Diameter of Tubes and Number of Tubes Required

The tube wall thickness is determined from the following equation:

$$t = 0.015 + pd/\Gamma^2 = 0.025 \text{ in.} \qquad (C1)$$

where 0.015 inch is the corrosion allowance in the tube wall, p is the operating pressure (200 lb/sq in.), and Γ is the allowable stress in the tube wall (2500 lb/sq in.). Thus, the outside diameter of the tubes d_o is 0.30 inch. The tube side flow area obtained from continuity is

$$A_f = w/\rho V = 0.936 \text{ sq ft}$$

and the flow area per tube is 0.000341 square foot. Thus, the number of tubes required N is 2745.

Shell Inside Diameter, Velocity, and Equivalent Diameter

Reference 25 presents a tube-count curve for tubes in a triangular pattern. Using this curve, the inside diameter of the heat exchanger shell is obtained. From figure B.4 of reference 25 for the design considered herein,

$$\frac{\text{Radius of tube bundle}}{\text{Tube pitch}} = \frac{R}{\lambda} = 39.0 \quad \text{for} \quad 2745 \text{ U-bend tubes}$$

Thus, R = 15.6 inches. The shell inside diameter is obtained from

Shell inside diam. = tube bundle diam. + tube diam. +

1.5 in. free space

= 33.0 in.

Thus, the shell cross-sectional area is 5.94 square feet. The total tube cross-sectional area (d_o = 0.30 in. and N = 5490) is 2.69 square feet. The shell-side flow area, then, is the difference between these two cross-sectional areas, or 3.25 square feet. For the U-bend heat exchanger considered herein, the shell-side velocity is 17.27 feet per second where the flow area used to determine this velocity is one-half of 3.25 square feet. The equivalent diameter for the shell side, d_e = (4)(flow area)/wetted perimeter, is 0.0542 foot.

Heat-Transfer Coefficients

The heat-transfer film coefficients for the shell side and tube side are determined as follows:

Film coefficient, shell side. - An empirical correlation for the shell side of baffled liquid-metal heat exchangers (ref. 22, p. 285) is used for the film coefficient on the shell side

$$Nu = 0.212\left[\left(d_e \times 12\ \frac{in.}{ft}\right)(Re)(Pr)\right]^{0.6} \qquad (C2)$$

where

$$Re = \rho V d_e/\mu = 512{,}000$$

and

$$h_{shell} = 7180\ Btu/(hr)(sq\ ft)(^{o}F)$$

Film coefficient, tube side. - The Martinelli-Lyon relation for liquid metals and a uniform wall heat flux is used for the film coefficient on the tube side (ref. 22, p. 73).

$$Nu = 7.0 + 0.025\left[(Re)(Pr)\right]^{0.8} \qquad (C3)$$

where

$$Re = 330{,}000$$

and

$$h = 18{,}950\ Btu/(hr)(sq\ ft)(^{o}F)$$

The over-all coefficient of heat transfer, based on outside surface, is calculated from the following equation (ref. 25),

$$\frac{1}{U_o} = \frac{d_o}{hd} + \frac{d_o \ln \frac{d_o}{d}}{k_m} + \frac{1}{h_{shell}} = 0.0002729 \qquad (C4)$$

and

$$U_o = 3670\ Btu/(hr)(sq\ ft)(^{o}F)$$

Heat-Transfer Surface Area

The following equations are used in determining the heat-transfer surface area:

$$Q = U_o S_h (\Delta T)_{ln} \tag{C5}$$

and

$$S_h = \pi d_o l N \tag{C6}$$

For this analysis, since $(wc_p)_{primary} = (wc_p)_{secondary}$, the log mean temperature $(\Delta T)_{ln}$ is simply the initial or final temperature difference ΔT, which is 100° R. Thus, using equations (C5) and (C6),

$$S_h = 818 \text{ sq ft}$$

and

$$l = 3.79 \text{ ft}$$

It is assumed that the heat-exchanger length (i.e., length of shell, tube sheet, and header) is 3.0 feet.

Sodium Pressure Drop Through Heat Exchanger

The pressure drops for both shell and tube side of the exchanger are determined from the Fanning friction pressure-drop formula.

$$\Delta p = \left(2.0 + f \frac{l}{d_e}\right) \frac{\rho V^2}{2g} \tag{C7}$$

The friction factor f is determined from reference 16 (p. 60). The constant 2.0 in equation (C7) allows for inlet, outlet, and U-bend losses in the respective circuits (ref. 25). The additional fluid pressure loss across baffles on the shell side is also considered to be included in the constant 2.0.

For the pressure drop through tubes, for Re = 330,000, f = 0.0145,

$$\Delta p = 20.1 \text{ lb/sq in.}$$

For pressure drop through shell, for Re = 512,000, f = 0.013,

$$\Delta p = 3.64 \text{ lb/sq in.}$$

Heat-Exchanger Weight

The weight of the 2745 U-bend tubes is determined from

$$W = \rho_m N l \frac{\pi}{4} (d_o^2 - d) = 993 \text{ lb} \qquad (C8)$$

The shell weight is determined by first calculating the shell outside diameter using equation (C1) to obtain the shell thickness. For the shell, a corrosion allowance of 0.020 inch was used. The shell thickness is 1.34 inches, and the shell outside diameter is 36 inches. Then, using equation (C8) the shell weight is 2162 pounds. Thus, the total heat-exchanger weight is 3155 pounds.

APPENDIX D

CONDENSER-RADIATOR ANALYSIS

Design Conditions

For a 20,000-kilowatt powerplant, the design conditions for the sodium condenser-radiator are as follows:

Total effective radiant surface area, A, sq ft	14,800
Fluid flow rate, w, lb/sec	53.0
Fluid inlet temperature, T, ^{o}R	1800
Fluid inlet pressure, p, lb/sq in.	2.72
Vapor saturation density at inlet, ρ_s, lb/cu ft	0.00394
Vapor mixture density at inlet, ρ_v, lb/cu ft	0.00502
Liquid density, ρ_l, lb/cu ft	48
Radiating tube wall thickness, t, in.	0.025
Supply pipe and header wall thickness, t, in.	0.125
Material density (stainless steel), ρ_m, lb/cu ft	494
Vapor velocity of sound (stagnation), C, ft/sec	2,265

Radiator Dimensions

A schematic diagram of the radiator configuration is shown in figure 9. The radiator is composed of two identical segments, and each segment is divided into four independent sections of equal plan form area, so that the tube diameter and wall thickness are constant within each section. The front-end tube length (l_1 = 13 ft) is prescribed from the half-cone angle of the shield $\beta = 3^{o}34'$ and the separation distance from the reactor. The over-all length of the radiator (dimension a in fig. 9) was obtained as

$$a = \frac{1}{\tan \beta}\left(\sqrt{l_1^2 + 2A \tan \beta} - l_1\right) = 192.2 \text{ ft} \qquad (D1)$$

where A is the plan form area of the segment (3700 sq ft). From the further condition that each segment is divided into four sections of equal plan form area,

$$a = \frac{1}{\tan \beta}\left(\sqrt{l_n^2 + 2A_n \tan \beta} - l_n\right) \qquad (D2)$$

and

$$l_{n+1} = l_n + a_n \tan \beta \qquad (D3)$$

The rear tube length is 25.0 feet, and the distance from the axis of rotation to the radiating tube inlet is 3 feet.

Radiating Tubes

Since the length of the individual radiating tubes varies within each section, the total weight of all tubes (both segments) is given by

$$W_t = 2\rho_m \pi \sum_{n=1}^{4} \sum_{j=1}^{N_n} l_j t_n d_{o,n} \left(1 - \frac{t}{d_o}\right)_n \tag{D4}$$

where N_n is the total number of tubes in each section of the radiator. Now, according to the assumed relation between effective radiating surface area and tube geometry,

$$\sum_{j=1}^{N_n} l_j d_{o,n} = A_n/2 \tag{D5}$$

where A_n is the total (both sides) effective radiating surface area of a tube section. With radiating surface area and tube wall thickness prescribed constant for all sections, the total tube weight for both segments becomes

$$W_t = \rho_m \pi A_n t \sum_{n=1}^{4} \left(1 - \frac{t}{d_o}\right)_n \tag{D6}$$

For rapid calculations, the weight can be determined with the use of an average value of diameter $\bar{d}_o$ as

$$W_t = \pi \rho_m t A (1 - t/\bar{d}_o) \tag{D7}$$

where A is the total required radiating surface area for the vehicle. The tube weight is thus a primary function of the tube wall thickness, the required radiating area, and the material density.

The tube inner diameter and the number of tubes in a given section are obtained from the radiator dimensions and the prescribed condition that the radiating surface area and sodium flow rate are the same in all sections, that is, $A_n/w_n = A/w = \text{constant}$. The radiating surface area for both sides of a section is given by

$$A_n = 2N_n \bar{l}_n d_{o,n} = 2N_n \bar{l}_n d_n (1 + 2t/d_n)$$

and the weight flow is given by

$$w_n = N_n \rho V \frac{\pi}{4} d_n^2$$

so that

$$\frac{A_n}{w_n} = \left(\frac{\bar{l}_n}{d_n}\right) \frac{8}{\pi} \frac{\left(1 + \frac{2t}{d_n}\right)}{\rho V} \tag{D8}$$

or

$$d_n = \frac{8\bar{l}_n}{\pi} \frac{(1 + 2t/d_n)}{\rho V(A/w)} \tag{D9}$$

The number of tubes in the section is then obtained from the width of the section a_n as

$$N_n = \frac{a_n}{d_n(1 + 2t/d_n)} \tag{D10}$$

For the entire radiator, a total of 1124 tubes is required.

Central Delivery Pipe

The weight of a section of delivery pipe is given in terms of its inner diameter as

$$W_{d,n} = \pi \rho_m d_n b_n t_n \left(1 + \frac{t}{d}\right)_n \tag{D11}$$

where

$$d_n = \sqrt{\frac{4}{\pi} \frac{2w_n}{\rho_{v,n} V_{v,n}}} \tag{D12}$$

where w_n is the fluid mass flow to each section (w/8). For the entire pipe length, with $t_n \rho_{v,n}$ and V_n constant,

$$W_d = \frac{2\sqrt{2\pi}\rho_m t}{\sqrt{\rho_v V_v}} \left[b_1 \sqrt{w_1} \left(1 + \frac{t}{d_1}\right) + b_2 \sqrt{w_2} \left(1 + \frac{t}{d_2}\right) + \right.$$

$$\left. b_3 \sqrt{w_3} \left(1 + \frac{t}{d_3}\right) + b_4 \sqrt{w_4} \left(1 + \frac{t}{d_4}\right) \right]$$

For equal fluid mass flow into each section, and for an average value of d, then,

$$W_d = 2\sqrt{\pi}\rho_m t \left[1 + \frac{t}{\bar{d}}\sqrt{\frac{w}{\rho_v V_v}}\left(b_1 + \sqrt{\frac{3}{4}}\,b_2 + \sqrt{\frac{1}{2}}\,b_3 + \sqrt{\frac{1}{4}}\,b_4\right)\right] \qquad (D13)$$

where w is the total flow rate.

Headers

Although shown as constant diameter sections in figure 9, the inlet and outlet headers were computed on the basis of a four-step reduction in diameter with equal lengths and equal reductions in flow rate. For the inlet header, the maximum diameter (at the center of the section) is determined to be that required to carry one-sixteenth of the mass flow, and the total weight of all inlet headers is obtained from

$$W_{h,i} = \frac{4\sqrt{\pi}\rho_m t(1 + t/\bar{d})}{\sqrt{\rho_v V_v}}\left(\frac{a}{4}\sqrt{\frac{w}{16}} + \frac{a}{4}\sqrt{\frac{3}{4}\frac{w}{16}} + \frac{a}{4}\sqrt{\frac{1}{2}\frac{w}{16}} + \frac{a}{4}\sqrt{\frac{1}{4}\frac{w}{16}}\right)$$

to give

$$W_{h,i} = \frac{\sqrt{\pi}}{4}\rho_m t(1 + t/\bar{d})a\sqrt{\frac{w}{\rho_v V_v}}\,(3.073) \qquad (D14)$$

For the outlet headers, the maximum diameter (at rear of section) is determined to carry one-eighth of the mass flow. Since the angle β is very small, the length of the outlet header in each section is practically equal to a_n, so that the total weight of the outlet headers is obtained as

$$W_{h,o} = \frac{\sqrt{2\pi}}{4}\rho_m t(1 + t/\bar{d})a\sqrt{\frac{w}{\rho_l V_l}}\,(3.073) \qquad (D15)$$

The weight of the connecting pipes between the header pipe and the outlet delivery pipe was computed from the required pipe diameter and length with a 50 percent additional allowance for the cutoff valves and flanges.

Radiator Surface Temperature

The relation between the temperature of the outer surface of the radiating tubes (radiating temperature) and the temperature of the condensing vapor flowing inside the tubes is obtained from consideration of the heat transfer across the tube wall. The heat released by the condensing vapor in the tube is

$$Q = wH_c \qquad (D16)$$

The heat transferred to the tube inner wall through convection is

$$Q = hS_h(T_s - T_w) \tag{D17}$$

and the heat transferred to the outer wall through conduction is

$$Q = \frac{k}{t} S_h(T_w - T) \tag{D18}$$

where T is the outer wall temperature. Solving for the outer wall temperature gives

$$T = T_s - \frac{wH_c}{S_h}\left(\frac{1}{h} + \frac{t}{k}\right) \tag{D19}$$

Since for the design considered herein the vapor velocity is very low, the vapor saturation temperature in equation (D19) is effectively equal to the vapor stagnation temperature. Thus, the radiator surface temperature can be directly related to the fluid temperatures considered in the cycle analysis. (For situations in which comparatively high vapor velocities are used, it may be desirable to check the magnitude of the difference between the static and stagnation states.)

In evaluating equation (D19) it is noted that the ratio of the tube heat-transfer area (inner surface area) to the radiating surface area (assumed as $2d_o l$) is very nearly $\pi/2$, so that

$$T = T_s - \left(\frac{w}{A}\right)\frac{2}{\pi} H_c \left(\frac{1}{h} + \frac{t}{k}\right) \tag{D20}$$

For the vapor temperature of 1800° R, with $H_c = 1518$ Btu per pound, $w = 9.55$ pounds per hour per kilowatt, $A = 0.74$ square foot per kilowatt, $t = 0.025$ inch, and $k = 14.7$ (austenitic stainless steel; linear extrapolation of data of ref. 23, p. 267), it is found that

$$T = T_s - 1.77 - 12{,}500/h \tag{D21}$$

where h is expressed in Btu per hour per square foot per $^\circ$F.

APPENDIX E

TURBINE DESIGN

The expansion through the turbine was assumed to be polytropic, that is,

$$pv^n = \text{Constant} \tag{E1}$$

The sodium vapor was assumed to satisfy the law

$$pv = X\frac{\overline{R}}{m}T \tag{E2}$$

In addition, the polytropic, or small-stage, efficiency of the turbine was assumed to have a constant value of 0.85 during the expansion process. The sodium vapor passing through the turbine was assumed, for the purpose of flow-area computation, to be monatomic. Mechanical design of the turbine rotor blades was limited by the centrifugal stress required to rupture the blades at the hub in 20,000 hours. The turbine-blade stress capabilities were taken from an extrapolation of the data in reference 26 for an arc-cast molybdenum alloy that contains 0.45 percent titanium and that has been stress relieved for 1 hour at 1800° F; the resulting values of limiting stress are shown in figure 10. Centrifugal stress at the hub radius of an untapered turbine rotor blade can be expressed as

$$\Gamma = \rho\Omega^2 A_f/2\pi g \tag{E3}$$

The rotor blades were considered to be tapered so that the stress is 0.7 of the stress without taper. Rotor-blade temperature at each axial station was assumed to equal local total temperature.

Required axial variation in annular flow area within the turbine was determined as a function of total temperature within the turbine by assuming that at each axial station the mass flow per unit annular area is 0.48 of the value that would choke the annulus if the gas tangential velocity were zero. Substitution of these values of flow area into equation (E3) permitted Γ/Ω^2 to be plotted as function of total temperature in figure 11. At the turbine exit, a higher proportion of choking flow is permissible than at other axial stations within the turbine; for this reason, the symbol in figure 11 representing turbine exit was located by choosing a mass flow per unit area that was 0.80 of the choking value.

Figures 10 and 11 can be used to establish at which axial station a combination of blade stress and temperature is limiting in the

following way: If these figures are superimposed with the temperature scales alined but with the ordinates displaced from one another, each relative displacement of the ordinates corresponds to a particular value of rotational speed Ω; this characteristic results from the fact that both ordinates are logarithmic. The conditions governing the relative offset of the ordinates are: (1) Allowable stress should always be at least as high as actual stress and (2) for effective design, the allowable and actual stresses should be equal at some point within the turbine. The selected superimposition of figures 10 and 11 is shown in figure 12. Rotor blade stress is shown to be more limiting at the turbine inlet than elsewhere. The resulting rotational speed Ω is 332 radians per second, or 3180 rpm.

Attainable works from turbines having various numbers of stages were estimated from an extension of reference 27 that incorporates tapering of the hub radius. For various turbine-exit radius ratios, the attainable work factors $-gJ\Delta h/U_h^2$ were determined for one- and two-stage turbines having an exit axial Mach number of 0.6 and a blade-row-inlet relative Mach number of 0.8. The increment in work factor resulting from changing from a one-stage turbine to a two-stage turbine was taken for each value of exit radius ratio as the increase in work factor associated with increasing the number of turbine stages by one; for each value of exit radius ratio, exit flow area was maintained at the value required to pass the mass flow, and the rotational speed was fixed at the required 332 radians per second. The resulting values of work factor are shown in figure 13 by solid lines.

The value of work factor required to produce the specified turbine work (357 Btu/lb) at the specified rotational speed (332 rad/sec) was determined for each of several values of exit radius ratio. The resulting relation between required work factor and exit radius ratio is shown in figure 13 by the dashed line. Any point of intersection of this dashed line with a solid line should be a satisfactory turbine design point. An exit radius ratio of 0.65 and four turbine stages were chosen as reasonable design conditions. At this value of exit radius ratio, the value of inlet radius ratio corresponding to figure 11 is 0.88; for the 64-inch turbine-tip diameter that corresponds to a power output of 20,000 kilowatts, the resulting blade height at the turbine inlet is 4 inches.

REFERENCES

1. Shepard, L. R., and Cleaver, A. V.: The Atomic Rocket. Jour. British Interplanetary Soc., vol. 7, 1948, pp. 185 and 234; vol. 8, 1949, pp. 23 and 59.

2. Spitzer, Lyman, Jr.: Interplanetary Travel Between Satellite Orbits. Jour. British Interplanetary Soc., vol. 10, no. 6, Nov. 1951, pp. 237-299.

3. Stuhlinger, Ernst: Electrical Propulsion Systems for Space Ships with Nuclear Power Source, pts. I-III. Jour. Astronautics, vol. 2, no. 4, 1955, pp. 149-152; vol. 3, no. 1, 1956, pp. 11-14; vol. 3, no. 2, 1956, pp. 33-36.

4. Van Allen, James A.: Scientific Uses of Earth Satellites. Univ. Mich. Press, 1956.

5. Rosenblum, Louis: Small Power Plants for Use in Space. Aero/Space Eng., vol. 17, no. 7, July 1958, pp. 30-33.

6. Moeckel, W. E.: Propulsion Methods in Astronautics. General Session of First Int. Cong. of Aero. Sci., Madrid (Spain), Sept. 13, 1958.

7. Glasstone, Samuel: Principles of Nuclear Reactor Engineering. D. Van Nostrand Co., Inc., 1955.

8. Rockwell, Theodore, III, ed.: Reactor Shielding Design Manual. TID-7004, AEC, Mar. 1956.

9. Kroeger, H. R.: Thermal Neutron Cross Sections and Related Data. NEPA Div., Fairchild Engine and Airplane Corp., Oak Ridge (Tenn.).

10. Chapman, G. T., and Storrs, C. L.: Effective Neutron Removal Cross Sections for Shielding. AECD-3978, AEC, 1955.

11. Schaefer, Hermann J.: Definition of a Permissible Dose for Primary Cosmic Radiation. Jour. Aviation Medicine, vol. 25, Aug. 1954, pp. 392-398; 411.

12. Whipple, Fred L.: The Meteoritic Risk to Space Vehicles. Presented at Int. Astronautical Cong., Barcelona (Spain), Oct. 6-12, 1957.

13. Huth, J. H., Thompson, J. S., and Van Valkenburg, M. E.: Some New Data on High Speed Impact Phenomena. Jour. Appl. Mech., vol. 24, no. 1, Mar. 1957.

14. Partridge, William S., Van Fleet, Howard B., and Whited, Charles R.: An Investigation of Craters Formed by High-Velocity Pellets. Tech. Rep. OSR-9. Dept. Elec. Eng., Univ. Utah, May 1957. (AD 132364.)

15. Whipple, Fred L.: Meteoric Phenomena and Meteorites. Ch. X of Physics and Medicine of the Upper Atmosphere, Univ. New Mexico Press, 1952, pp. 137-170.

16. Hogerton, J. F., and Grass, R. C., eds.: The Reactor Handbook. Vol. 2. Engineering. AECD-3646, AEC, May 1955.

17. Gaffert, Gustaf A.: Steam Power Stations. McGraw-Hill Book Co., Inc., 1940, p. 523.

18. Inatomi, T. H., and Parrish, W. C.: Thermodynamic Diagrams for Sodium. NAA-SR-62, AEC, July 13, 1950.

19. Sheldon, Lucian A.: Thermodynamic Properties of Mercury Vapor. Preprint No. 49-A-30, ASME, 1950.

20. Pitzer, Kenneth S., et al.: The Volumetric and Thermodynamic Properties of Fluids. II - Compressibility Factor, Vapor Pressure, and Entropy of Vaporization. Jour. Am. Chem. Soc., vol. 77, no. 13, July 5, 1955, pp. 3433-3440.

21. Getman, Frederick H., and Daniels, Farrington: Outlines of Physical Chemistry. Seventh ed., John Wiley & Sons, Inc., 1941, p. 24.

22. Jackson, Carey B.: Liquid Metals Handbook - Sodium(NaK) Supplement. TID 5277, July 1, AEC, 1955.

23. Hogerton, J. F., and Grass, R. C.: The Reactor Handbook. Vol. 3. Sec. 1 - General Properties of Materials. AECD-3674, AEC, Mar. 1955.

24. Pugh, J. W.: The Tensile Properties of Molybdenum at Elevated Temperatures. Trans. Am. Soc. Metals, vol. 47, 1955, pp. 984-1001.

25. Davies, R. W., et al.: 600 MW Fused Salt Homogeneous Reactor Power Plant. CF-56-8-208, AEC, Aug. 1956.

26. Freeman, Robert R., and Briggs, J. Z.: Molybdenum for High Strength at High Temperatures. Jet Prop., vol. 27, no. 2, pt. 1, Feb. 1957, pp. 138-147.

27. Cavicchi, Richard H., and English, Robert E.: A Rapid Method for Use in Design of Turbines Within Specified Aerodynamic Limits. NACA TN 2905, 1953.

TABLE I. - HEAT-EXCHANGER SUMMARY

[Electrical power, 20,000 kw; reactor thermal power, 88,000 kw.]

Performance		
	Shell side	Tube side
Fluid circulated	Radioactive liquid sodium	Nonradioactive liquid sodium
Weight flow, lb/sec	1235	1235
Temperature (in), ^{o}R	2800	2475
Temperature (out), ^{o}R	2575	2700
Operating pressure, lb/sq in.	200	200
Velocity, ft/sec	17.1	30
Pressure drop, lb/sq in.	3.64	20.1
Transfer rate design	3670 Btu/(hr)(sq ft)(^{o}F)	

Construction	
Tubes	Outside diam., 0.30 in.; Inside diam., 0.25 in.; length, 3.79 ft; number, 2745; pitch, 0.40; weight, 993 lb
Shell	Outside diam., 36 in.; Inside diam., 33 in.; length, 3.0 ft, (includes allowance for tube sheet and headers); weight, 2162 lb

TABLE II. - DESIGN SUMMARY OF NUCLEAR TURBOELECTRIC POWERPLANT FOR SPACE VEHICLE

Electrical power output, kw	20,000
System efficiency	0.227
Reactor thermal power, kw	88,000
Turbine adiabatic efficiency	0.85
Generator efficiency	0.95
Reactor pressure drop, lb/sq in.	8.0
Radiator pressure drop, lb/sq in.	12.5
Heat-exchanger pressure drop, shell side, lb/sq in.	3.64
Heat-exchanger pressure drop, tube side, lb/sq in.	20.10
Reactor-inlet temperature, ^{o}R	2575
Reactor-outlet temperature, ^{o}R	2800
Heat-exchanger inlet temperature, ^{o}R	2475
Heat-exchanger outlet temperature, ^{o}R	2700
Turbine-inlet temperature, ^{o}R	2500
Radiator-inlet temperature, ^{o}R	1800
Reactor coolant (sodium) flow rate, lb/sec	1235
Sodium vapor flow rate, lb/sec	53
Reactor core size, in. diam. × in. length	30×30
Reflector thickness, in.	3.0
Number of fuel assemblies in reactor	28
Fuel plates per fuel assembly	21
Spacing between fuel plates, in.	0.12
Moderator and reflector material	Beryllium-Oxide
Fuel	Uranium-235

TABLE III. - SYSTEM WEIGHTS FOR ELECTRIC POWER OUTPUT

OF 20,000 KILOWATTS

Reactor plus one additional loading	4,860
Heat exchanger	3,155
Pumps	600
Evaporator	135
Shield	24,500
Neutron shield, 7500 lb	
Gamma shield, 17,000 lb	
Turbine	10,500
Generator	12,140
Radiator (primary)	42,750
Radiator (generator cooling)	2,500
Piping	11,700
Structure	2,500
Sodium loading plus 1000 lb spare	4,000
Total powerplant weight, lb	119,340

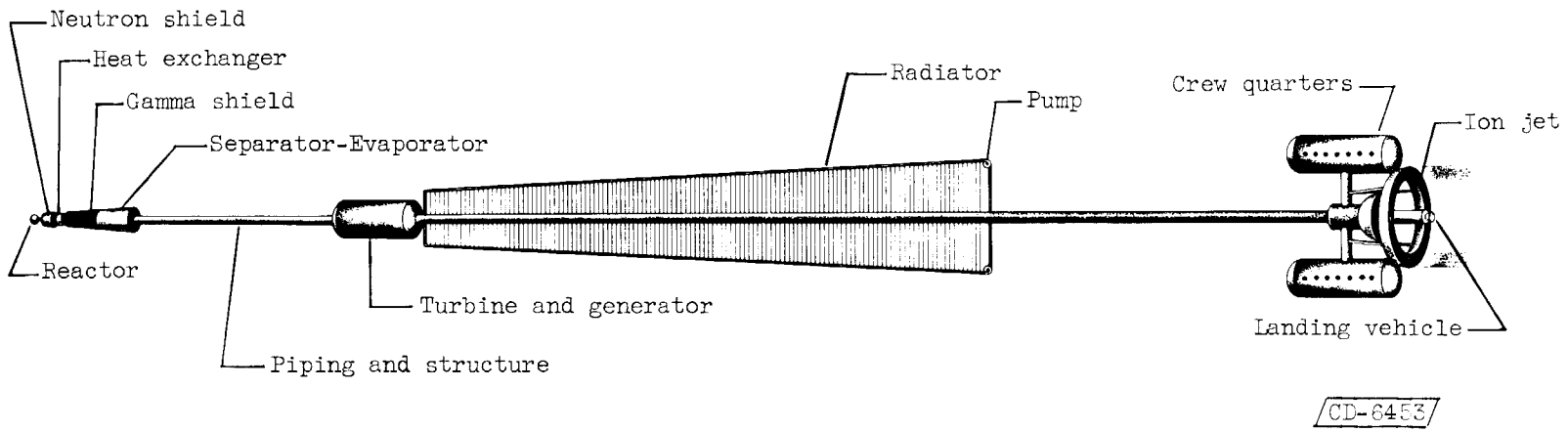

Figure 1. - Space-vehicle configuration.

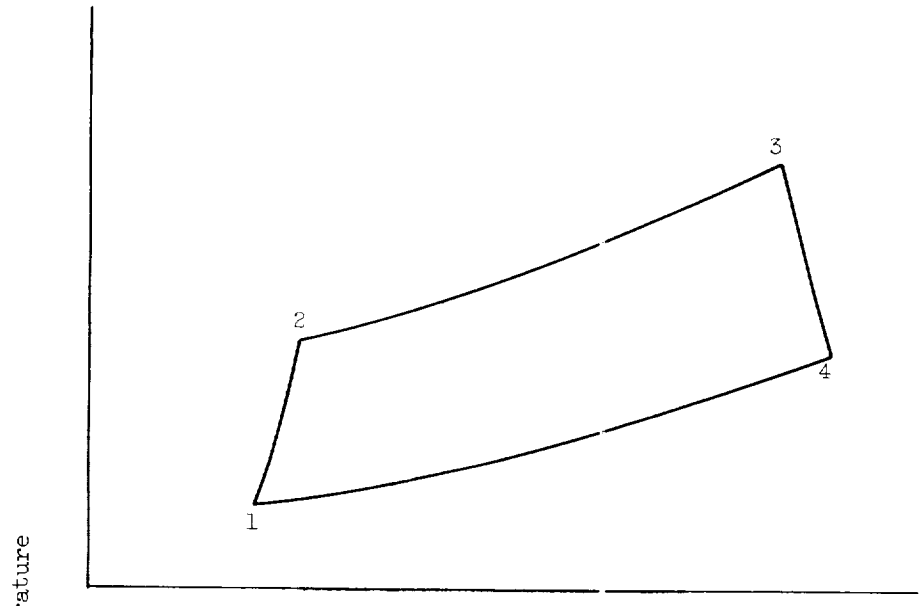

(a) Gas cycle.

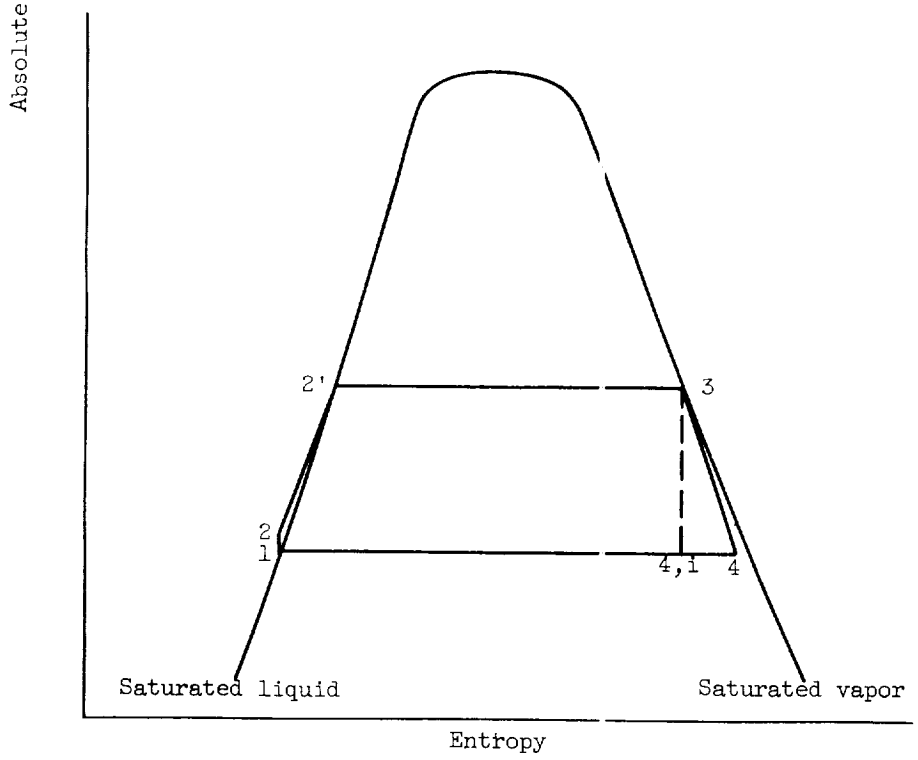

(b) Vapor cycle.

Figure 2. - Temperature-entropy diagrams for gas and vapor thermodynamic cycles.

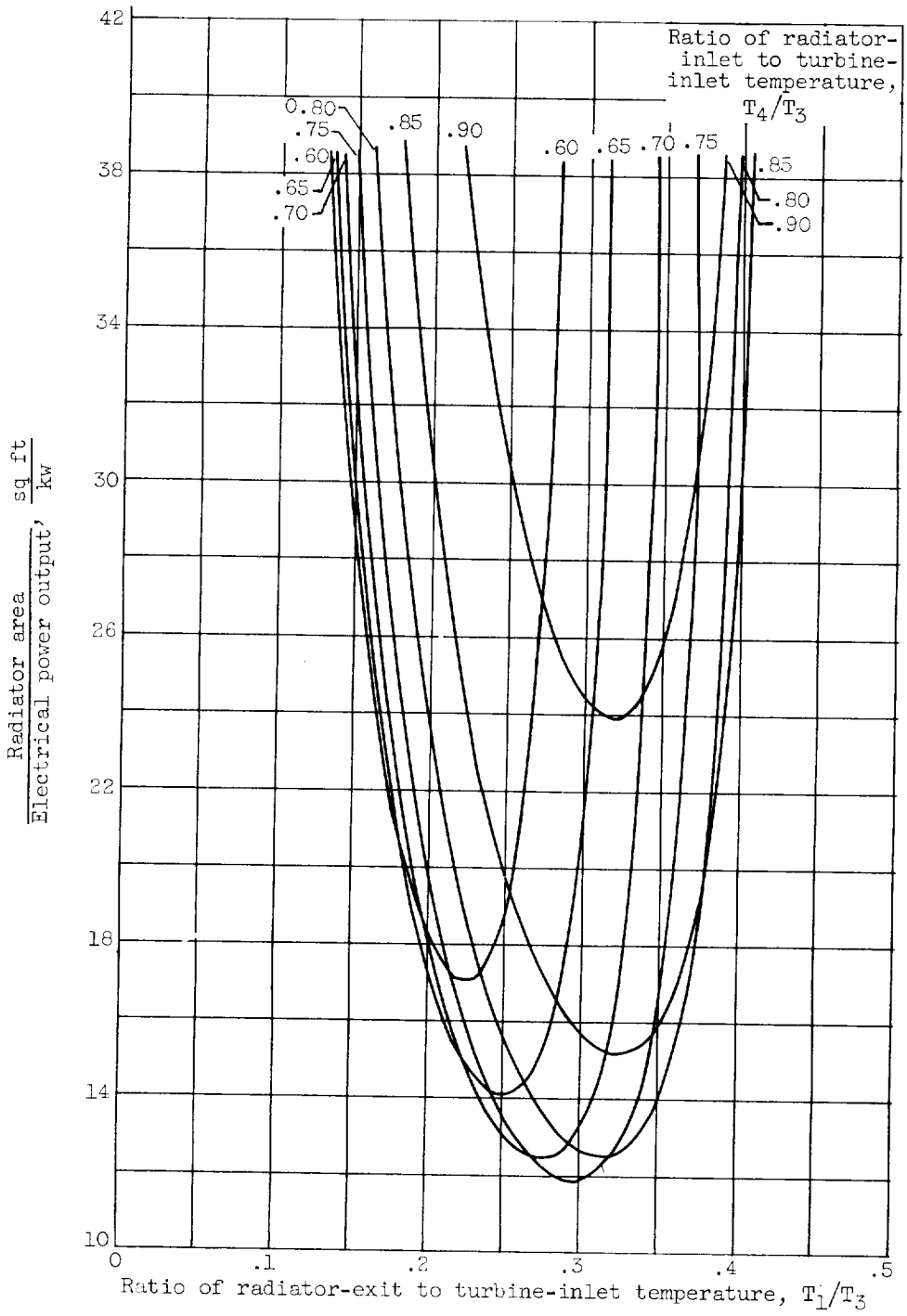

Figure 3. - Typical plot showing effect of cycle parameters on radiator area per kilowatt for gas cycle. Turbine-inlet temperature, T_3, 2500° R; emissivity, ε, 0.90; generator times mechanical efficiency, η_g, 0.95; ratio of specific heats, 1.66; component efficiency, $\eta_C = \eta_T = 0.80$; pressure ratio, $p_3/p_2 = p_1/p_4 = 0.95$.

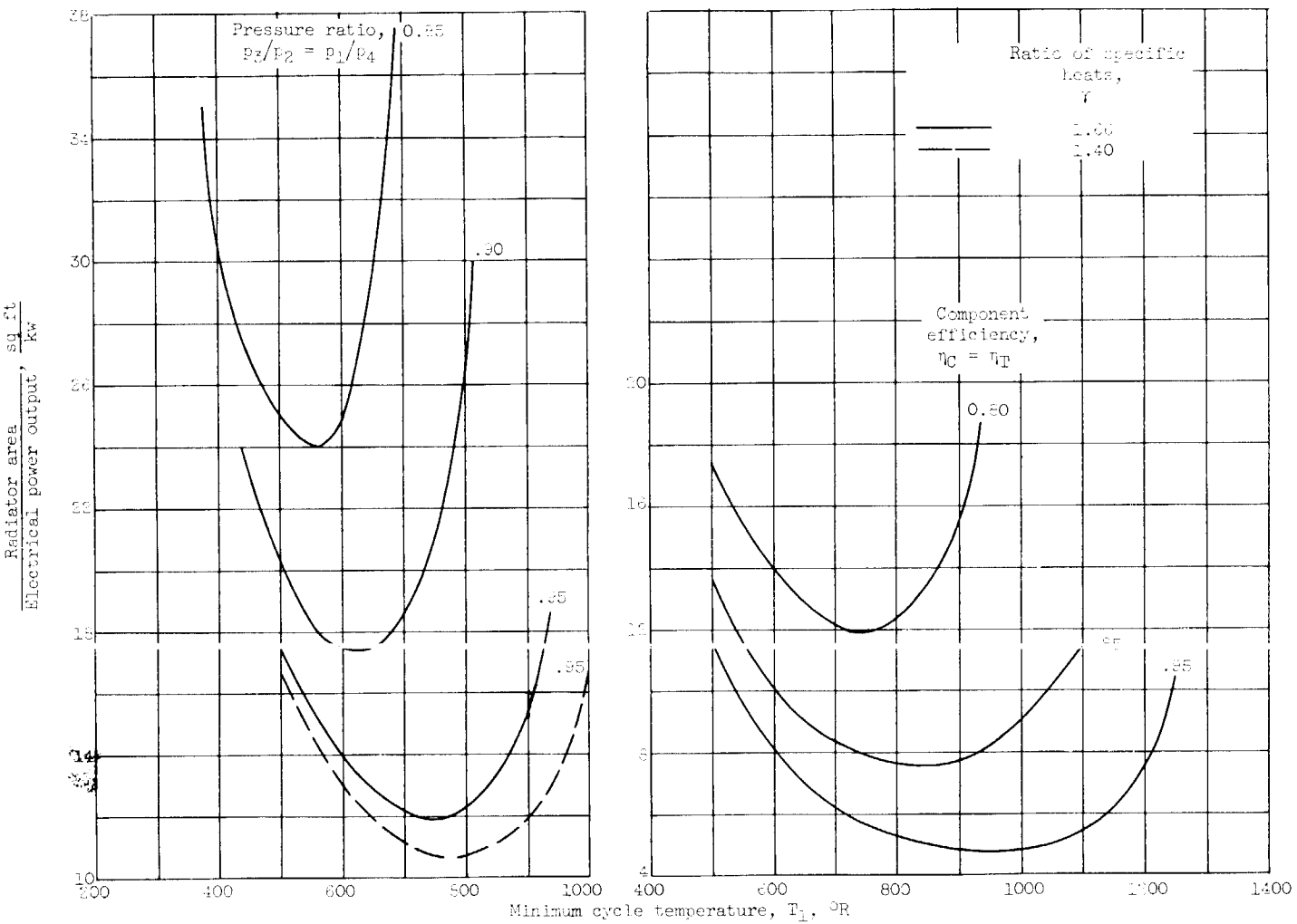

(a) Effect of pressure ratio and ratio of specific heat. Component efficiency, $\eta_C = \eta_T = 0.80$.

(b) Effect of compressor and turbine efficiency, ratio of specific heat, 1.00; pressure ratio $p_3/p_2 = p_1/p_4 = 0.95$.

Figure 4. - Effect of various parameters on radiator area per kilowatt for gas cycle. Maximum cycle temperature, 2500° R.

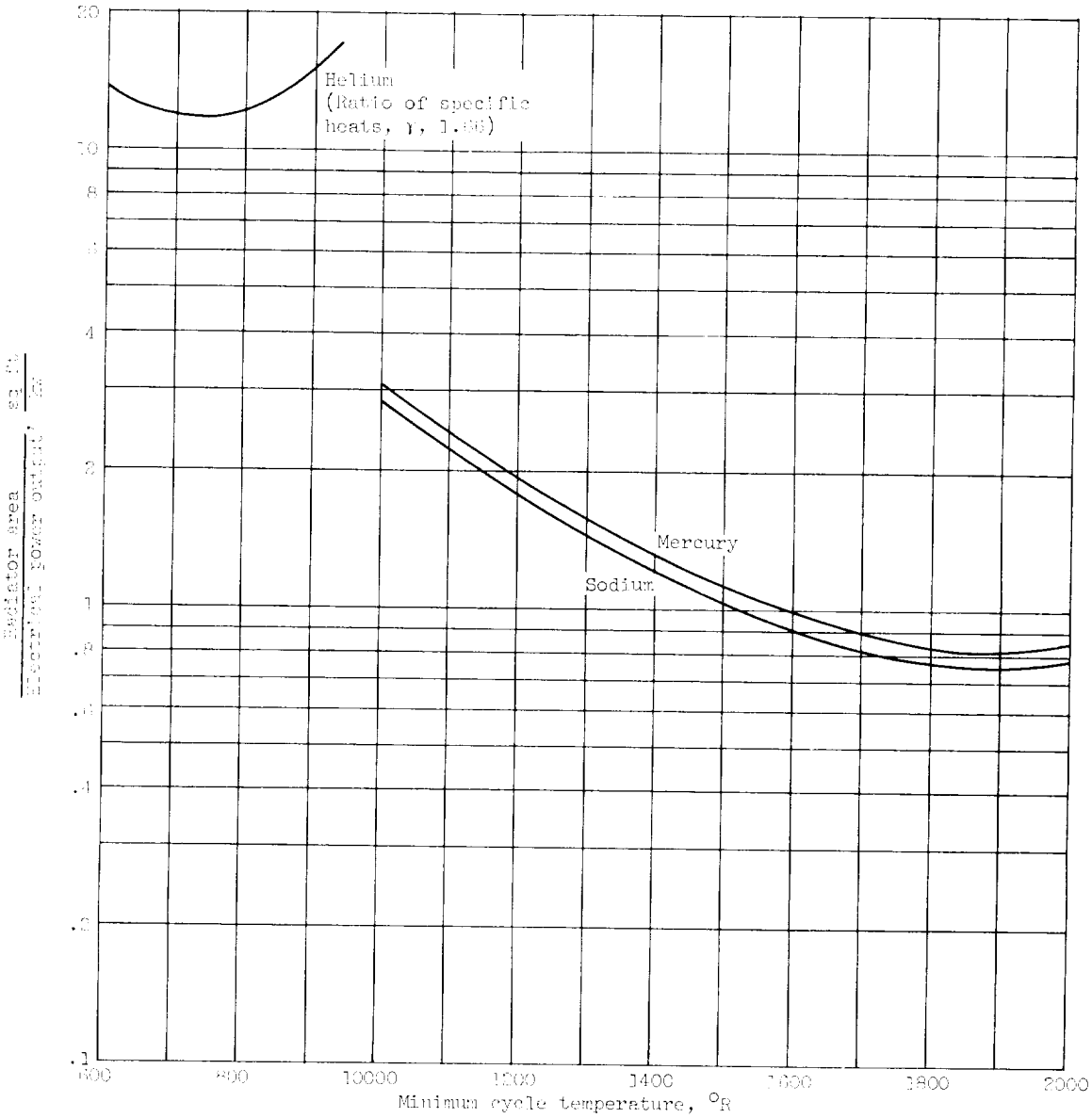

Figure 5. - Comparison of radiator area per kilowatt for gas (helium) and vapor (mercury and sodium) cycles. Turbine-inlet temperature, T_3, 2500° R; component efficiencies, $\eta_C = \eta_T$, 0.80.

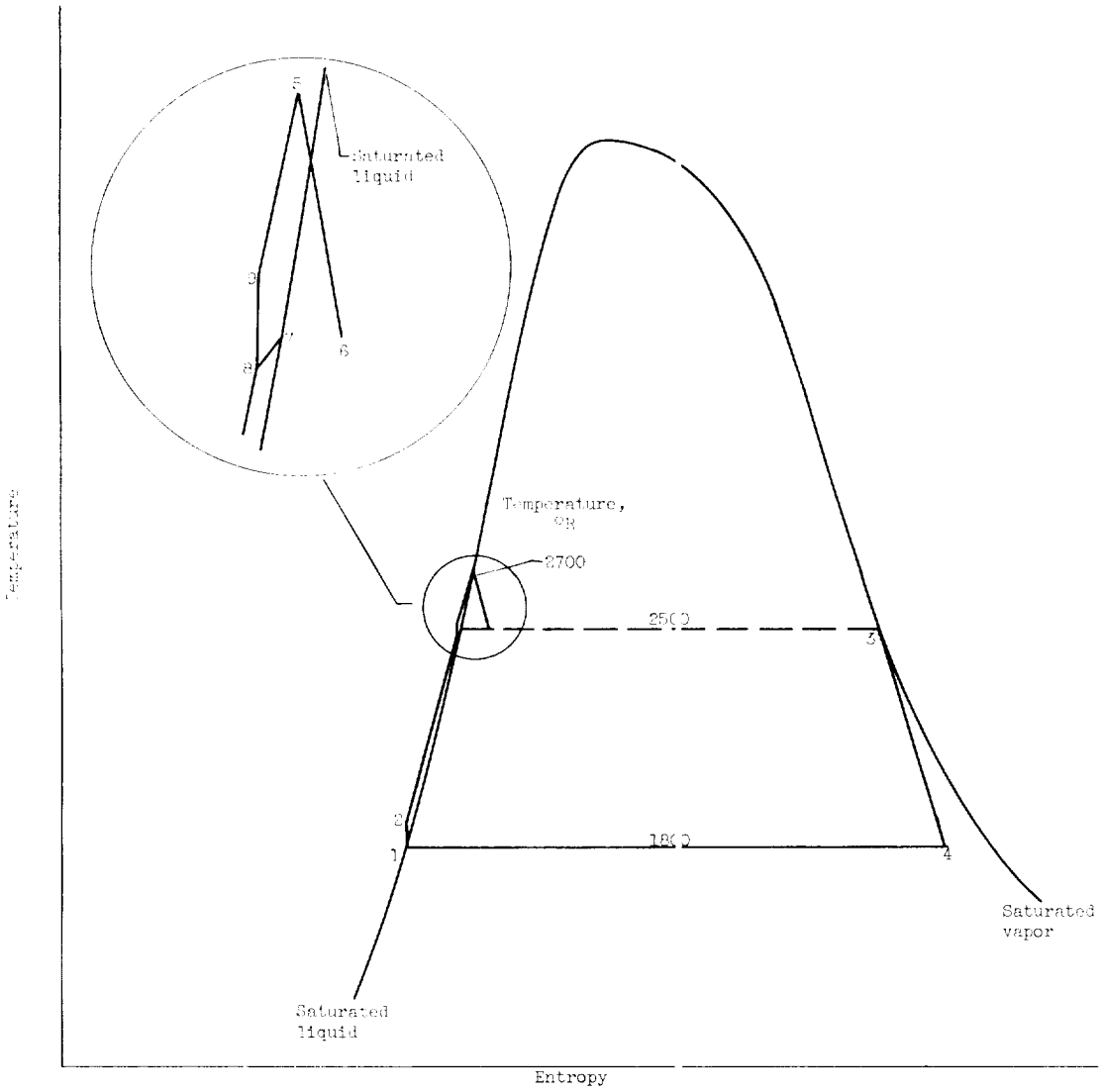

Figure 8. - Temperature-entropy diagram for 20,000-kilowatt nuclear turboelectric powerplant using sodium as working fluid.

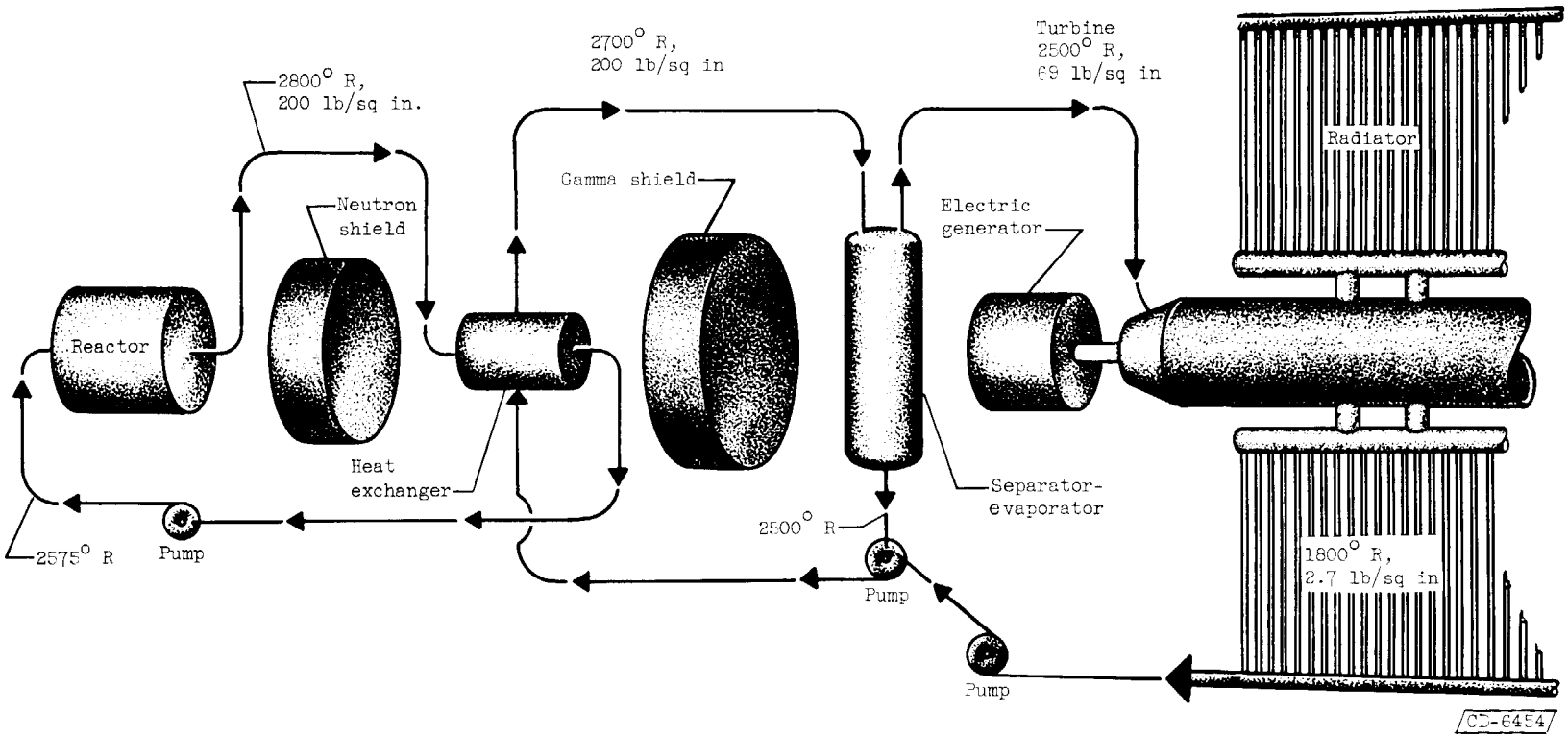

Figure 7. - Schematic arrangement of sodium cycle.

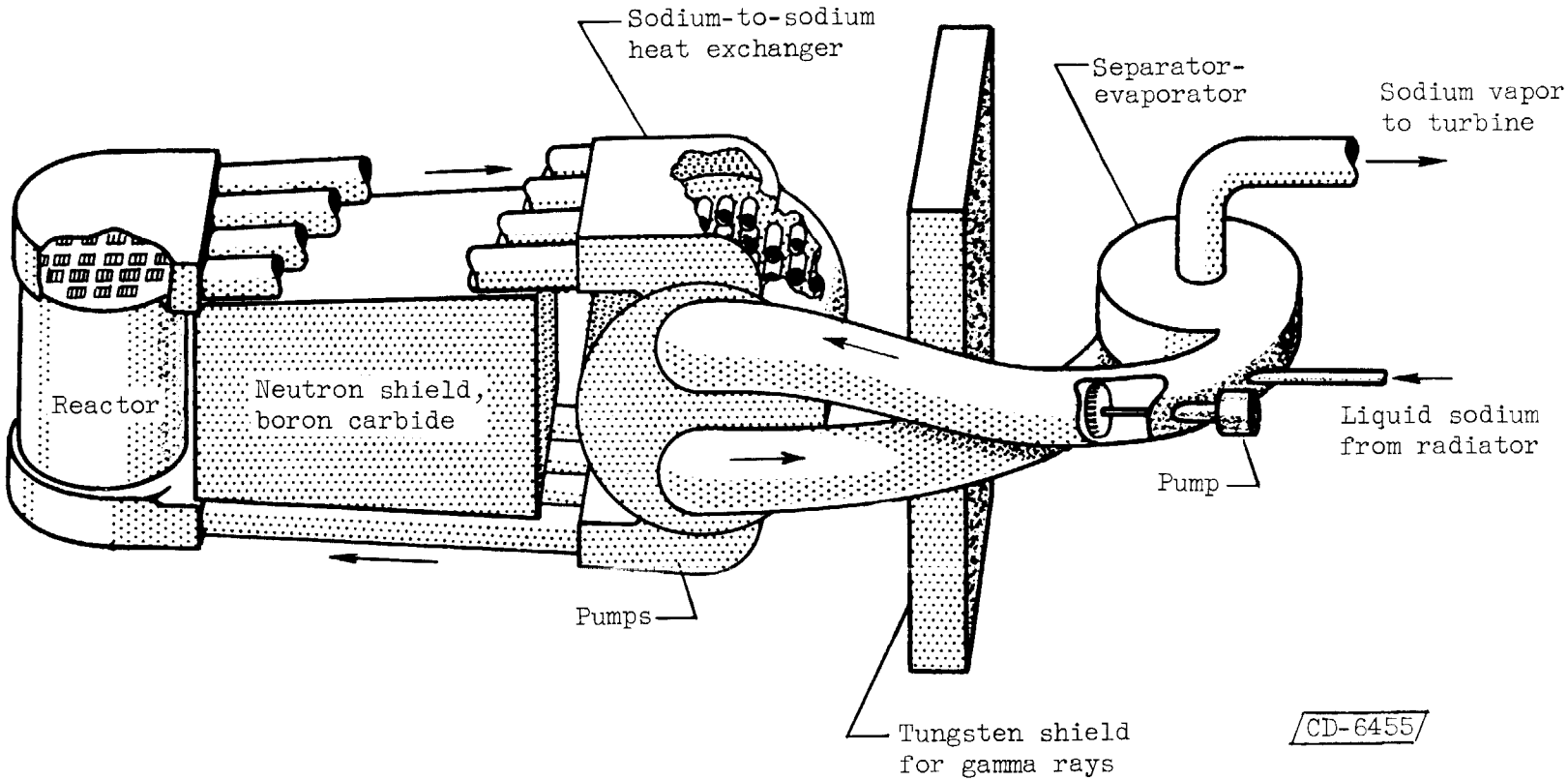

Figure 8. - Reactor end of powerplant.

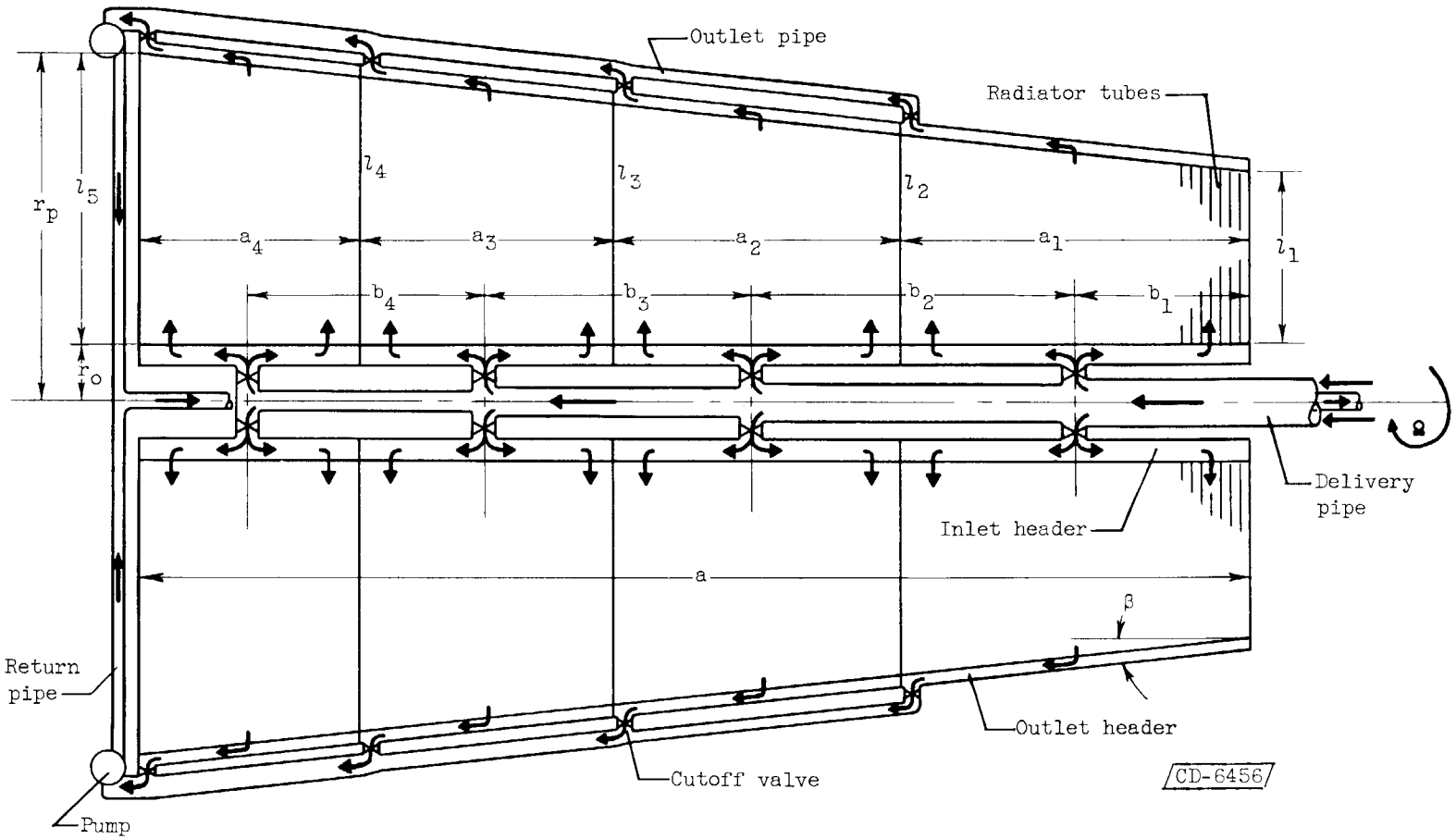

Figure 9. - Schematic diagram of condenser-radiator showing components, flow directions, and principal dimensions. (Drawing not to scale.)

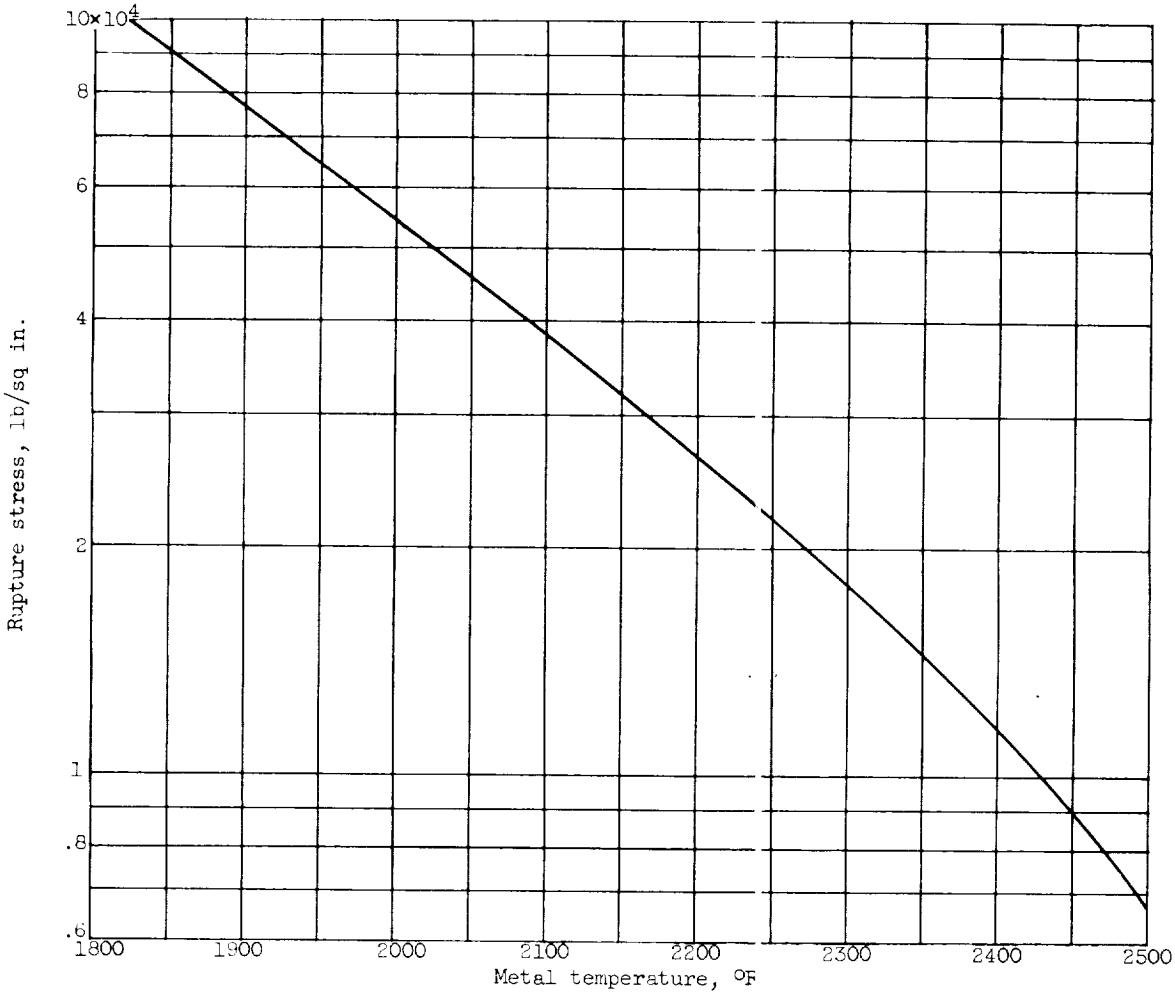

Figure 10. - Stress to rupture for 0.45 percent titanium-molybdenum alloy in 20,000 hours (ref. 26).

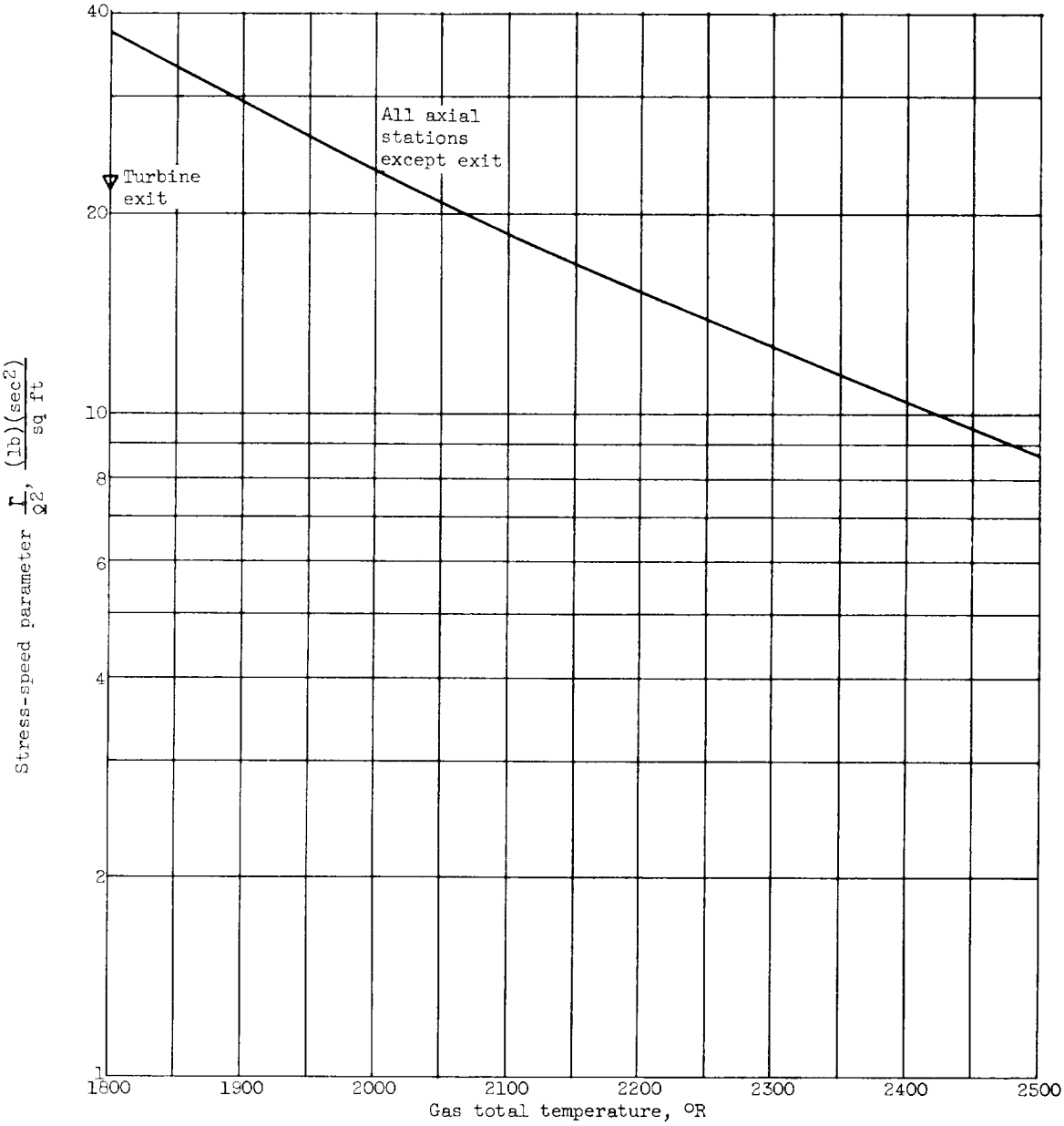

Figure 11. - Stress-speed parameter determined from flow-area requirements of turbine for sodium-vapor powerplant at 2500° R.

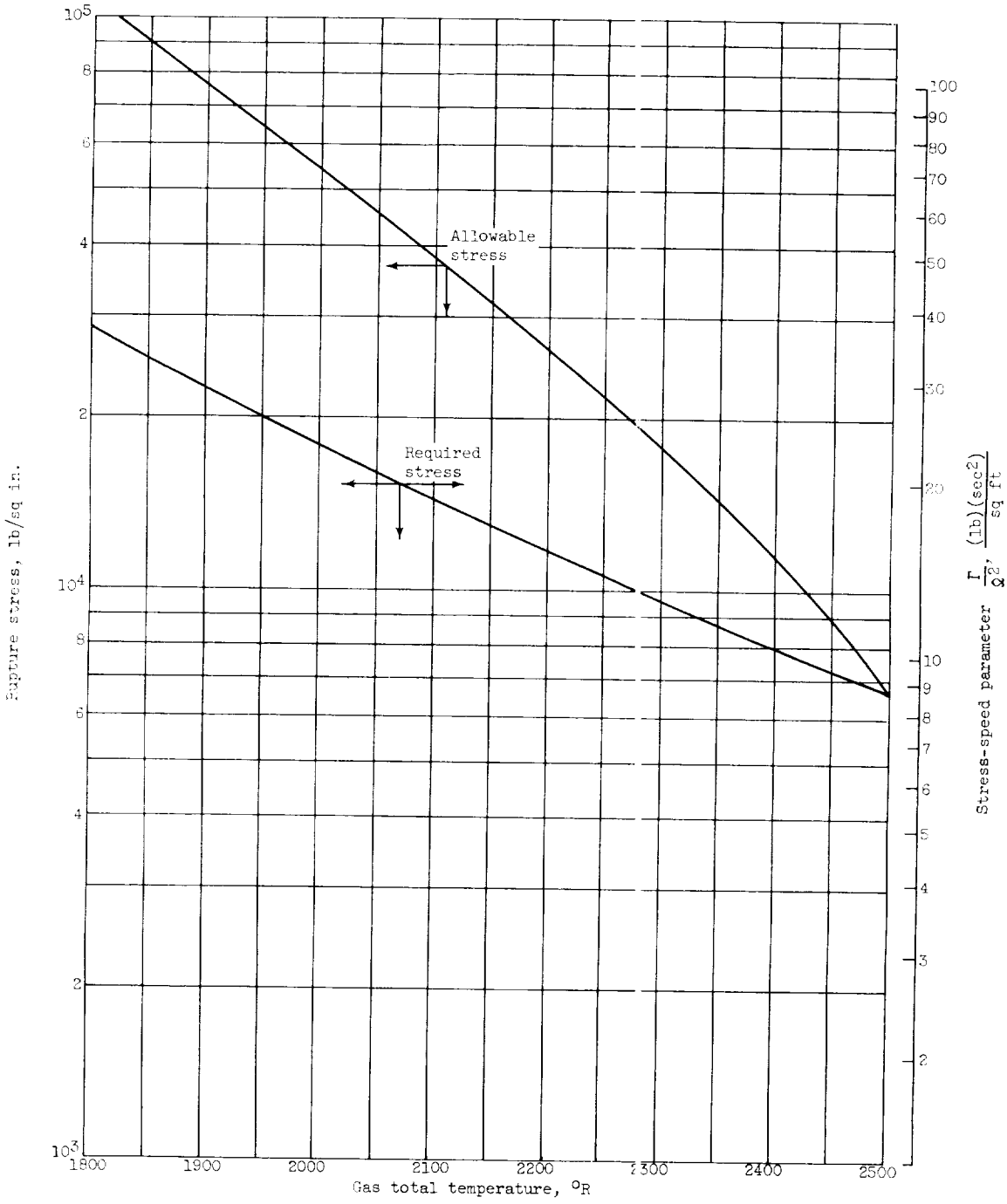

Figure 12. - Relation of allowable and required stress showing that critical stress-temperature condition exists at turbine inlet. Resulting rotational speed, 332 radians per second.

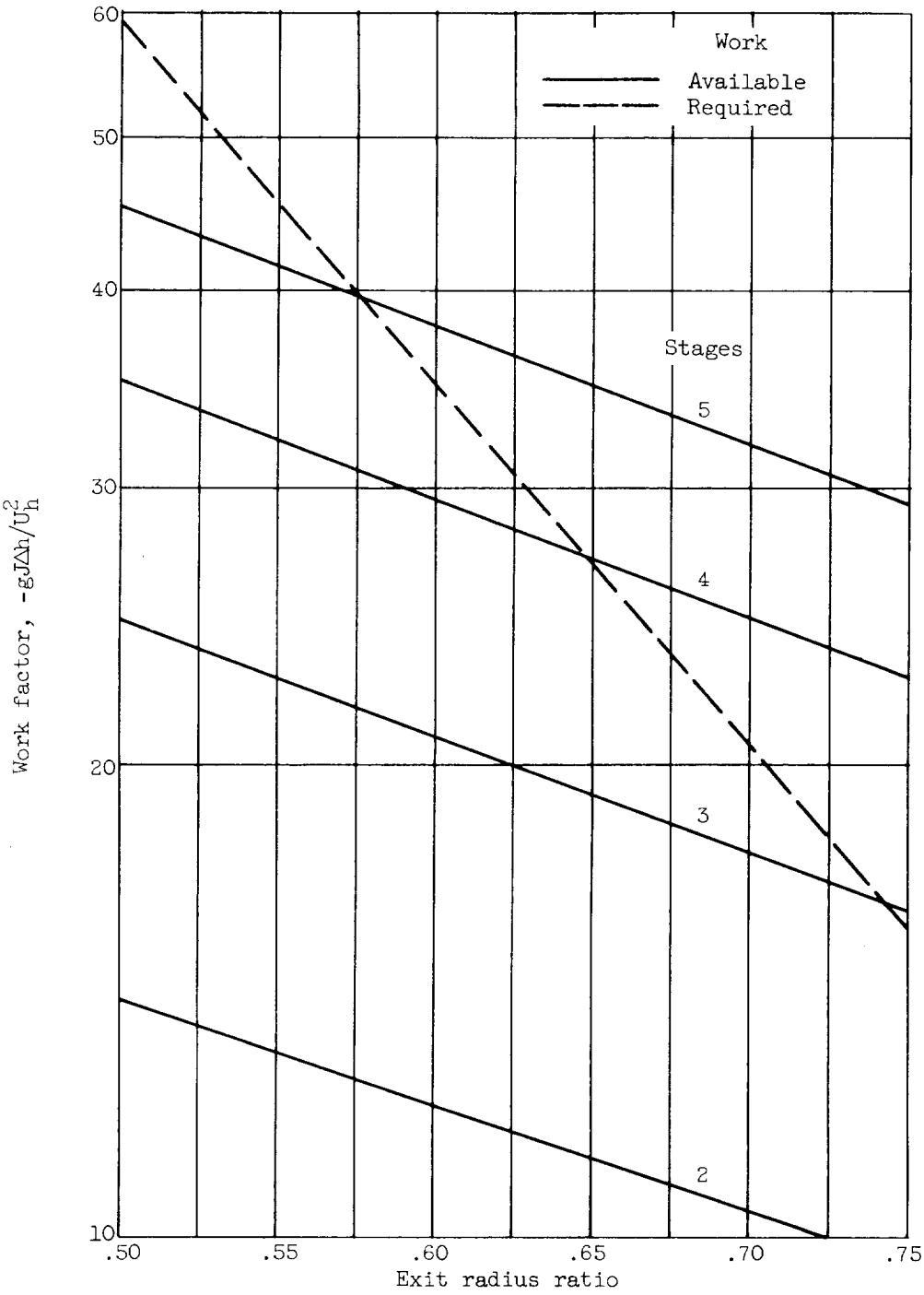

Figure 13. - Comparison of required and available turbine work for various numbers of turbine stages. Exit area, 12.88 square feet; rotational speed, 332 radians per second; specific work, 357 Btu per pound; inlet temperature, 2500° R; working fluid, sodium.